Journal of Marine Research, 55, 633–670, 1997

The hydrography and circulation of the upper 1200 meters in the tropical North Atlantic during 1982–91

by Gennady Chepurin[1] and James A. Carton[1]

ABSTRACT

We assemble a collection of 7591 conductivity-temperature-depth stations in the tropical Atlantic between 5S and 20N for the period 1982–1991 using data from the Soviet SECTIONS program enhanced by contributions primarily from the WESTRAX and FOCAL/SEQUAL programs. Most of the stations are west of 30W, forming a series of 21 surveys. In addition there were five multi-ship basinwide surveys, each taking 1.5–3 months to complete. The quality of the SECTIONS data is discussed and comparisons between the data sets are shown. Within the pycnocline, southern water is distinguished by salinity that is 0.3 psu lower than its northern counterpart at the same density. This difference allows us to distinguish the origin of pycnocline water. Based on this information together with geostrophic analysis we confirm that much of the water transported across the equator in the North Brazil Current retroflects eastward south of 8N. In summer and fall the water of the North Brazil Current merges with the water of the North Equatorial Current to form the North Equatorial Countercurrent, whose axis shifts southward with depth. East of 35W part of the mass transport in the Countercurrent is lost to the equatorial zone, while the rest continues eastward. During winter and spring eastward currents are found in two latitude bands, a surface current between 5–10N and a weaker current south of 5N confined to the thermocline. This latter North Equatorial Undercurrent has no surface expression in winter. During the summer and fall the northern boundary of Southern Hemisphere water at pycnocline depths is given by the North Equatorial Countercurrent. During the rest of the year the northern boundary of Southern Hemisphere water only penetrates to the edge of the weaker North Equatorial Undercurrent south of 5N.

The availability of ten years of data allows us to examine aspects of year-to-year variability. Among these results the data set reveals strong meandering of the North Equatorial Countercurrent between 42W and 35W during the summer of 1987. The meandering also appears in contemporaneous Geosat altimetry. Another unusual feature occurred in the summer 1986 when there was a strong thermocline current transporting water northward at the rate of 26 Sv. Water mass analysis shows that this current was the result of a pressure gradient set up by an intrusion of warm low-salinity water from the Southern Hemisphere. The fact that this high transport occurred in the interior ocean suggests that interior flows must be monitored during any attempt to observe meridional transports of mass or heat.

1. Introduction

The purpose of this paper is to examine the temperature, salinity, and geostrophic velocity in the upper 1200 m of the northern tropical Atlantic. This layer plays an important

1. Department of Meteorology, University of Maryland, College Park, Maryland, 20742, U.S.A.

role in the general circulation of the oceans because it is here that warm water crosses into the Northern Hemisphere.

Estimates of the northward transport of warm water are fairly consistent. Schmitz and Richardson (1991) estimated the volume transport of southern water entering the Florida Current to be 13 Sv (13×10^6 m^3/s). At the equator Schott *et al.* (1995) suggest that the western North Brazil Current alone transports 12 Sv of southern water northward at levels above $\sigma_\theta = 26.8$. Once across the equator the fate of this southern water is much less certain. Many studies have shown that only a few Sverdrups of water flows continuously along the South American coast (Korotaev and Chepurin, 1989; Candela *et al.,* 1992; Wilson *et al.,* 1994). An additional 3–4 Sv moves northward in the form of anticyclonic eddies spun off the North Brazil Current (Fratantoni *et al.,* 1995). The remaining 6 Sv that crosses the equator in the west apparently enters the zonal circulation system. The mechanisms by which these flows of southern water move northward are the subjects of this paper.

The mean and seasonal circulation in the upper layers has been the subject of extensive efforts in the past 20 years (e.g., Merle, 1978; Cochrane *et al.,* 1979; Katz, 1981; Garzoli and Katz, 1983; Richardson and Reverdin, 1987; Molinari and Johns, 1994). Despite these efforts some basic questions remain. In the western basin the motion field is dominated by the seasonal appearance of the eastward North Equatorial Countercurrent (NECC). An eastward North Equatorial Undercurrent (NEUC) is also apparent in and below the thermocline, as suggested by Cochrane *et al.* (1979) and Molinari and Johns (1994). But, the relationship between these two currents remains unclear. Much of the hydrographic data previously analyzed was confined to restricted areas. Because of the presence of strong seasonal and interannual variability, the eastward extension of these currents still remains to be defined. Perhaps most important, limitations in the total amount of data have prevented previous studies from examining year-to-year changes in the circulation of this region.

In this paper we examine the extensive hydrographic record for the ten-year period 1982–1991. Part of the data comes from two experiments, FOCAL/SEQUAL[2] (1060 stations), and WESTRAX[3] (172 stations). The first of these data sets and an additional 355 stations were obtained from the World Ocean Atlas (Levitus, 1994). In this study these data have been enhanced by 4931 stations collected as part of the Soviet program SECTIONS,[4] the largest hydrographic experiment ever conducted in the tropical Atlantic.

Because most of our data come from SECTIONS (Efimov, 1987) and have not been extensively documented in the western literature, Section 2 presents this data set. Fortunately, some overlap exists between this data set and the WESTRAX data set allowing us to make some temperature and salinity comparisons. In Section 3 we examine

2. Programme Francais Ocean et Climat dans l' Atlantique Èquatorial (FOCAL) Seasonal Response of the Equatorial Atlantic Experiment (SEQUAL)
3. WESTern TRopical Atlantic eXperiment
4. Soviet Short-term Climate Variability Program, also known by the Russian acronym RAZREZI

ocean properties along two meridional sections. One of these is at 44W and represents conditions in the western basin. The other is at 23W and represents conditions in the central basin. In Section 4 the data are presented along constant density surfaces. In the late-1980s some surveys allow us to examine water properties for the whole basin. Otherwise we are restricted to analysis of properties either in the western or central basin.

2. Data sources and processing

By far the largest data set ever collected in the tropical Atlantic was collected as part of the Soviet SECTIONS program. The six ships used during SECTIONS were provided by two different oceanographic laboratories. The Marine Hydrophysical Institute (MHI) of the Ukrainian Academy of Science in Sevastopol supplied two research vessels for the experiment, *Academic Vernadsky* and *Mikhael Lomonosov,* as well as providing overall coordination. The State Oceanographic Institute (SOI) of the USSR supplied the *Volna, Jakov Gakkel, Dmitry Ushakov,* and *Parshin.* The hydrographic stations from MHI research vessels were recorded at 5 m vertical resolution with 65% extending to a depth of 1200 m. The data from SOI research vessels were collected at 10 m resolution, but were archived in MHI only at 16 standard levels. The common hydrographic data set was archived in MHI and is the source of the data we report on here. The data set consists of 4931 temperature and salinity profiles collected during 26 surveys carried out during 1984–1990 (listed in Table 1). The 26 surveys were divided into three stages.

During the first stage, 1984–1985, eight hydrographic surveys were conducted near the South American coast between 2S to 20N. Each survey consisted of 8–10 hydrographic sections made perpendicular to the coast. The spacing between the sections was 100 km, while the station spacing along each section was 50 km. The objective of this stage was to define the seasonal cycle of variations in the northwest (Efimov, 1987).

During the second stage, 1986–1988, 12 surveys were carried out between 2S–12N latitude and 58W–5W longitude. During the first two years the sections were oriented north-south, with 166 km spacing between tracks and 55 km along track spacing. In 1988 the spacing between tracks increased to 333 km. During this stage generally two or three research vessels were collecting data simultaneously. The objective of stage two was to investigate seasonal variability of the NECC (Bulgakov *et al.,* 1989).

The third stage, 1989–1990, had seven surveys organized into three experiments designed to sample the synaptic variability. Two experiments were carried out in the west and one in the central basin. In the first, carried out in the spring of 1989, two research vessels were present simultaneously in the western region. *Dmitry Ushakov* collected data from west to the east, while *Academic Vernadsky* collected data from east to the west. The second experiment was carried out in the east during the fall 1989 by *Jakov Gakkel* and *Academic Vernadsky.* The third experiment was carried out in the west during the winter of 1990. The cruises were carried out using the *Parshin* and *Academic Vernadsky.*

Vertical profiling by the research vessels of MHI was done with two conductivity-temperature-depth (CTD) probes, MHI-4102 and MHI-4201. Both were constructed at

Table 1. Summary of cruises in the tropical Atlantic.

Experiment	Start	End	No. of stations
FOCAL/SEQUAL	07/06/82	07/23/82	52^
FOCAL/SEQUAL	10/13/82	11/21/82	97^
FOCAL/SEQUAL	01/11/83	02/18/83	153^
FOCAL/SEQUAL	03/16/83	04/29/83	95^
FOCAL/SEQUAL	07/01/83	08/06/83	237^
FOCAL/SEQUAL	10/03/83	12/02/83	126^
FOCAL/SEQUAL	01/11/84	02/15/84	94^
FOCAL/SEQUAL	04/02/84	05/14/84	102^
FOCAL/SEQUAL	07/03/84	08/07/84	104^
SECTIONS (Ac. Ver.)	08/11/84	11/20/84	279
SECTIONS (J. Gak.)	10/28/84	12/09/84	133
SECTIONS (Ac. Ver.)*	01/21/85	02/26/85	167
SECTIONS (Ac. Ver.)*	03/15/85	04/06/85	111
SECTIONS (Voln.)	03/15/85	05/15/85	328
SECTIONS (Ac. Ver.)	06/22/85	07/10/85	164
SECTIONS (Ac. Ver.)	07/30/85	09/14/85	160
SECTIONS (J. Gak.)!	07/30/85	09/14/85	151
SECTIONS (M. Lom.)*	03/15/86	05/05/86	168
SECTIONS (Ac. Ver.)	03/28/86	04/24/86	219
SECTIONS (Voln.)**	03/28/86	05/04/86	209
SECTIONS (M. Lom.)	07/16/86	09/16/86	298
SECTIONS (Ac. Ver.)	09/03/86	10/25/86	207
SECTIONS (Voln.)	02/07/87	03/26/87	298
SECTIONS (Ac. Ver.)	02/09/87	04/03/87	300
SECTIONS (Ac. Ver.)*	06/04/87	07/22/87	288
SECTIONS (M. Lom.)!	06/18/87	08/06/87	200
SECTIONS (M. Lom.)	05/21/88	09/14/88	168
SECTIONS (Ac. Ver.)	07/29/88	09/14/88	198
SECTIONS (Ac. Ver.)	04/25/89	06/05/89	82
SECTIONS (D. Ush.)!	05/03/89	06/02/89	161
SECTIONS (J. Gak.)	09/07/89	10/02/89	79
PREWESTAX (M. Bal.)	08/28/89	09/16/89	53^
SECTIONS (Ac. Ver.)	10/15/89	10/29/89	75
SECTIONS (Ac. Ver.)	11/07/89	11/28/89	99
WESTRAX (M. Bal.)	01/01/90	02/19/90	33
SECTIONS (Par.)	02/08/90	03/08/90	119
SECTIONS (Ac. Ver.)	02/08/90	04/14/90	270
WESTRAX (M. Bal.)	09/17/90	10/04/90	38
WESTRAX (M. Bal.)	01/16/91	01/30/91	25
WESTRAX (M. Bal.)	06/20/91	07/03/91	42
WESTRAX (M. Bal.)	09/07/91	09/17/91	14

*—salinity is being corrected by bottle data.

**—salinity is being corrected by closest calibrated hydrographic data.

^—data from WOA-94 (Levitus, 1994).

!—salinity cannot be corrected.

MHI and tested by the state testing agency using standard methods (Kalashnikov, 1985). The first instrument has an accuracy of $\pm 5 \times 10^{-4}$ Siemens/m, ± 0.025°C and $\pm 3 \times 10^{-2}$ Mpa at the 95% level. The rosette surrounding the MHI-4102 holds 16 bottles. During the cruises these bottles were used to take the samples of water at standard levels for nutrient analysis. This instrument has higher conductivity error levels of $\pm 2.5 \times 10^{-3}$ Siemens/m. The MHI-4201 was designed to be used while the ship is underway, and thus does not carry water bottles.

The vertical resolution of the MHI-4102 is one meter. During the cruises the profiles were smoothed with a 5-m cosine filter, and the data were saved at 5 m intervals. The vertical resolution of the MHI-4201 depends on ship velocity, but is typically 1–2 m. The data from this instrument were smoothed and saved at 5 m intervals as well. The surface value of salinity and temperature represents the first measured value, and has not been smoothed. The depth of the first measurement varied between 5–15 m. The data presented here were collected while the CTD was descending.

Temperature and salinity observations for different cruises were compared with each other and with climatologies of Levitus and Oort (1977), Levitus (1994), and Chernova and Chmutov (1987). Based on these comparisons we identified some problems with the salinities. We find the most severe problem with the MHI salinities was an error due to lack of onboard calibration. The calibration error had the effect of elevating salinities during five cruises, *Academic Vernadsky* 1/21/85–2/16/85, 3/15/85–4/6/85, and 6/4/87–7/22/87, and *Mikhael Lomonosov* 3/15/86–5/5/86 and 6/18/87–8/6/87 (throughout this paper we will use dates to identify particular cruises). For depths greater than 600 m the increase was typically 0.03 psu. Unfortunately, this error depends on depth and varies from cruise to cruise. Nevertheless, the error is an order of magnitude smaller than average difference in salinity between Northern and Southern Hemisphere origin waters (Fig. 5). Thus we are still able to use salinity to separate these water types. For the three cruises of *Academic Vernadsky* and for *Mikhael Lomonosov* 3/15/86–5/5/86 bottle samples had been collected and salinity had been determined by titration. For these cruises we developed an empirical correction to salinity observations. For *Mikhael Lomonosov* 6/18/87–8/6/87 we were unable to make such a correction. This cruise covered a unique part of a basinwide survey, and so the data were used in our analysis. The figure legends indicate where it is used.

The SOI research vessels used *hydrozond* or *zondbathometer* CTD probes. These two probes have identical error characteristics: $\pm 3 \times 10^{-3}$ Siemens/m, ± 0.03°C, and $\pm 5 \times 10^{2}$ Mpa at the 95% level, all estimated in the same way as MHI data. The calculation of salinity from conductivity was carried out by engineers aboard the research vessels. Unfortunately three of the cruises, *Jakov Gakkel* 7/30/89–9/17/89, *Volna* 3/28/86–5/4/86, and *Dmitry Ushakov* 5/3/85–6/2/85 also had salinity calibration problems. The inaccuracies are most evident below 600 m where the profiles are typically 0.03 psu too high. No bottle data were available for these cruises. However one cruise, *Volna* 3/28/86–5/4/86, was a part of a larger-scale transatlantic survey by three research vessels. Thus we were able to correct salinity for this cruise by comparing profiles on constant density surfaces

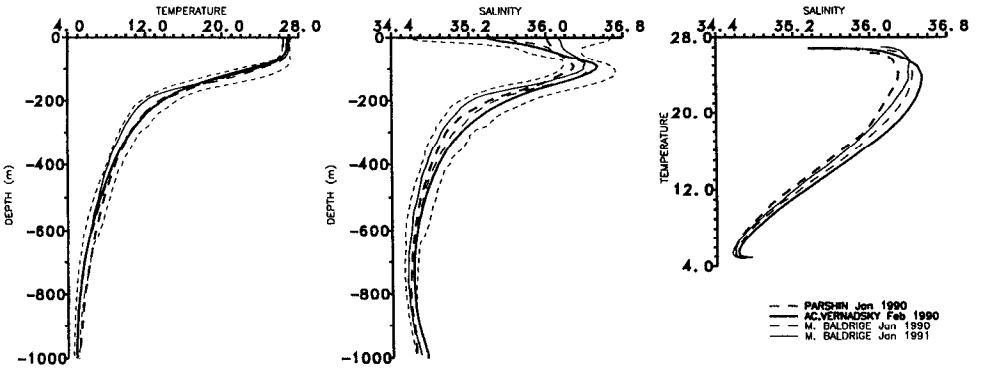

Figure 1. Hydrographic profiles (at 0N, 44W) from a SECTIONS cruise on February 23, 1990 and a WESTRAX cruise on February 11, 1990. (a) Temperature with depth, (b) salinity with depth, (c) temperature versus salinity.

with neighboring calibrated profiles. Data from the other two cruises were not used in this study.

As pointed out in the Introduction, SECTIONS immediately preceded the 1990–1991 surveys of the WESTRAX experiment (Johns and Wilburn, 1993). We begin our presentation of results by comparing the temperature and salinity profiles from SECTIONS and WESTRAX stations in January, 1990 (Figs. 1–3). In Figure 1 a SECTIONS profile near 0N, 44N from *Academic Vernadsky* 2/8/90–4/14/90 is compared with a profile from the WESTRAX cruise *Malcolm Baldrige* 1/1/90–2/19/90 carried out 12 days earlier. During those 12 days the thermocline and halocline apparently rose 60 m, but the temperature-salinity relationship remained the same. In another example, a station from the same *Malkolm Baldrige* cruise is compared with one from *Parshin* 2/8/90–4/14/90 at 9N 52W (Fig. 2). Here the SECTIONS salinities are 0.05 psu lower for the same temperature in the

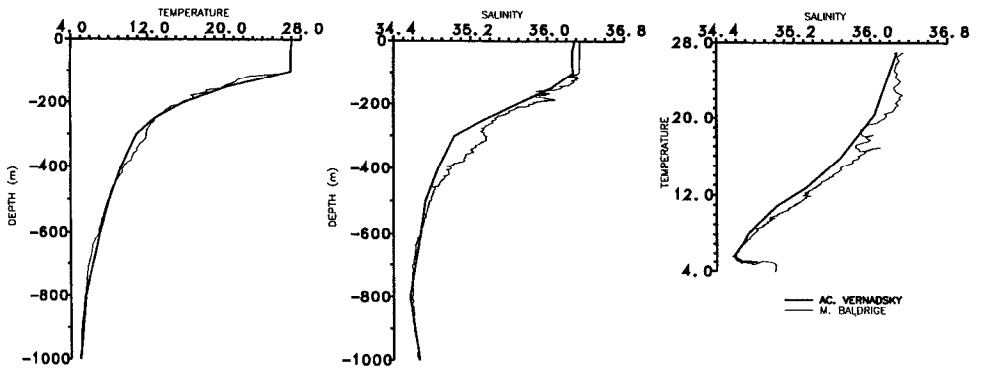

Figure 2. Hydrographic profiles from a SECTIONS cruise on February 12, 1990 and a WESTRAX cruise on February 4 at 9N, 52W. (a) Temperature with depth, (b) salinity with depth, and (c) temperature versus salinity.

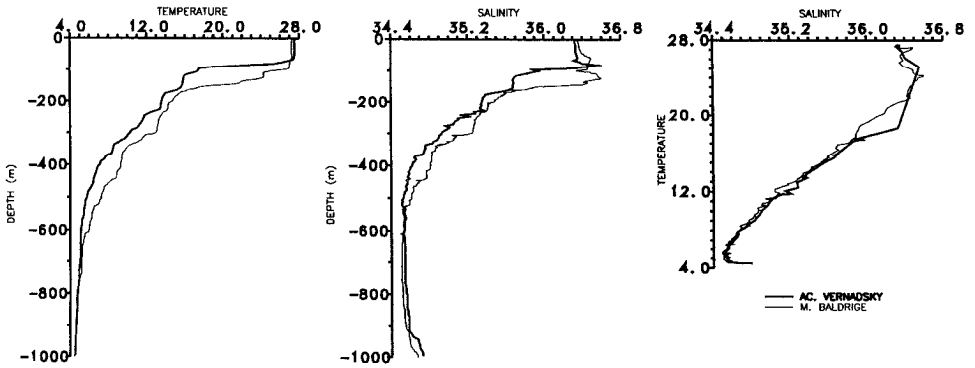

Figure 3. Comparison of average temperature versus salinity for a WESTRAX cruise and a SECTIONS cruise in the area of overlap between the surveys for January–February, 1990. The average of a WESTRAX cruise a year later is added to illustrate the year-to-year changes. (a) Temperature versus depth, (b) salinity versus depth, (c) temperature versus salinity. Dashed lines in (a) and (b) indicate the root-mean-square profile deviations of the combined data set.

upper 500 m layer than the WESTRAX salinities, although the time difference was only 8 days. This change in salinity between the stations may be the result of the intense eddy activity we observe in this location, or it may indicate error. The average temperature and salinity profiles from two WESTRAX and two SECTIONS cruises in the same western region and season are compared in Figure 3. The averages are indistinguishable from one another. This result, along with comparisons with individual profiles and with the climatologies convinces us that there is no systematic calibration problem in our SECTIONS data, although the accuracy may be lower than reported above.

To make our analysis as comprehensive as possible we conducted a search of the World Data Center archive for other station data during the period. The search excluded data near the coast in water shallower than 200 m. This search identified 2660 CTD stations of which 638 were contributed by FOCAL (discussed above). The spatial distribution of the combined data set shown in Figure 4a. The greatest concentration occurs in the northwest with more than 75% west of 35W (5802 stations). The vertical distribution of the data is shown in Figure 4b. In the upper 600 m we have over 7000 stations. This number decreases rapidly below 1000 m, so that by 1200 m we have only 65% of the quantity of data available at the surface. Based on this data distribution our analysis focuses on the water properties of the upper 1200 m. For information about deep and bottom water processes the reader is urged to turn to other studies such as Friedrichs and Hall (1993) and Richardson and Schmitz (1993). The temporal distribution of the station data is shown in Figure 4c. Data from 1982–1983 come mainly from FOCAL, while data after 1984 come mainly from SECTIONS. The seasonal distribution is fairly homogeneous. The minimum data, 1225, occurs during fall (September–November), and the maximum, 2804, during summer (June–August).

Water properties are more nearly uniform along constant potential density surfaces than

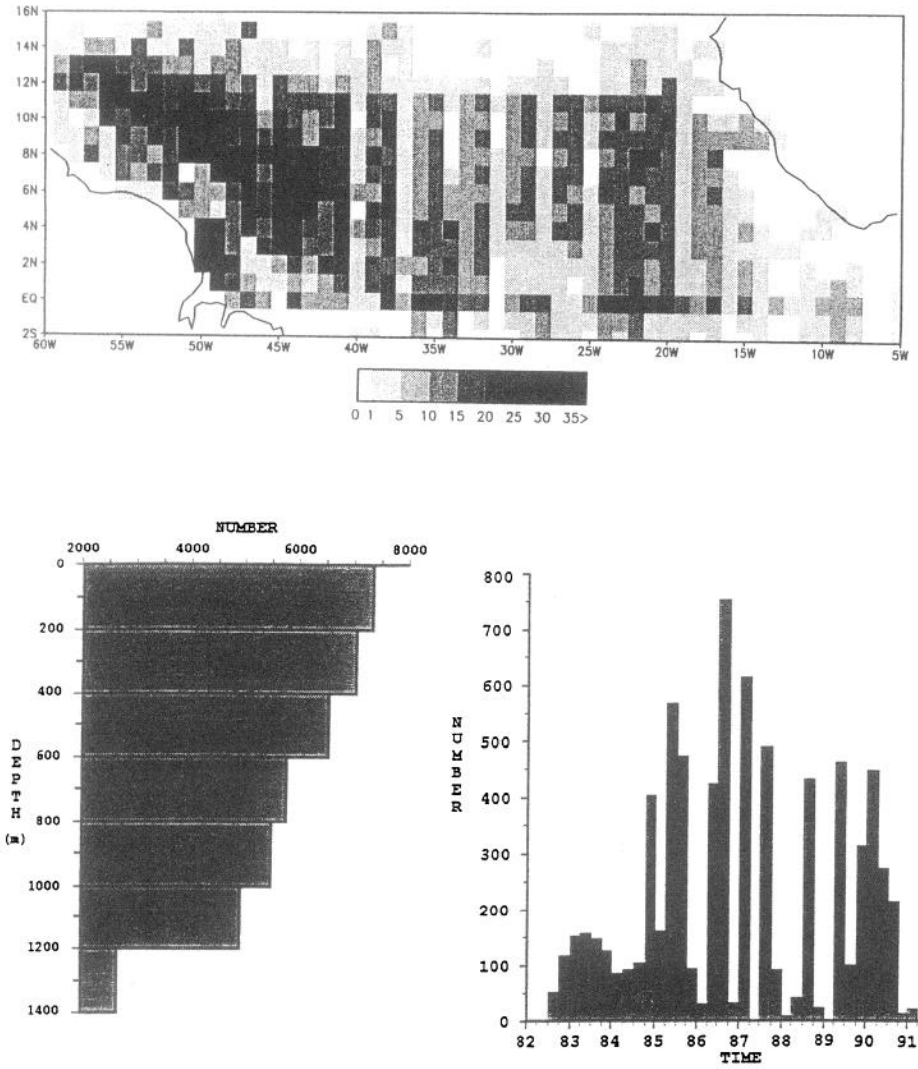

Figure 4. (a) Station data distribution 1982–1991, (b) distribution of observations with depth, 1982–1991, (c) distribution of observations with time, 1982–1991.

along pressure surfaces. Here we follow the common oceanographic convention and evaluate properties along σ_θ surfaces, which represent an approximation to potential density surfaces. We evaluate σ_θ using the international equation of state for sea water (EOS-80). The maximum error in σ_θ based on the published instrumental accuracies is $\pm 3.4 \times 10^{-6}$ kg m^{-3}. In fact most of the error in the seasonal analyses is an error of representativeness due to unresolved physical processes. We calculated this error based on spatial-temporal spectral estimations reported in Korotaev and Chepurin (1989). These

authors conclude that the error variance is 20% of the observation variance. For σ_θ this gives us an estimate of $\pm 9 \times 10^{-5}$ kg m^{-3} within the pycnocline and $\pm 10^{-5}$ kg m^{-3} at lower depths. For each station the depth of constant σ_θ surfaces was determined by cubic spline interpolation. The error of the pressure calculations for the MHI data is 4.2 db for the $\sigma_\theta = 24.5$ surface and 8.5 db for the $\sigma_\theta = 26.8$ surface. The same interpolation procedure was used to calculate temperature and salinity on the potential density surfaces. We estimate the total error at each station to be 0.06 psu and 0.56°C in the pycnocline and 0.03 psu and 0.09°C below it.

Because we intend to work on constant σ_θ surfaces we compute a pressure anomaly stream function according to:

$$\psi_a - \psi_r = \delta_a P'_a - \delta_r P'_r - \int_{P_r}^{P_a} \delta dP,$$

where $P'_r = P_r - \overline{P_r}$, $\overline{P_r}$ is the area-average pressure on a surface of constant $\sigma_{\theta r}$, δ is anomaly of specific volume, and where the subscripts a and r indicate the surface of interest and the reference surface. McDougall (1989) has pointed out a difficulty in defining a stream function on a constant σ_θ surface. However, Zhang and Hogg (1992) have shown that the error introduced is small as long as the slopes of the isopycnal surfaces are not large. Because our observations extend only to 1200 m it was decided to assume a reference level at the interface between Antarctic Intermediate Water (AAIW) and North Atlantic Deep Water (NADW). This interface, as indicated below, occurs at $\sigma_\theta = 27.6$. The average depth of this surface is 956 ± 9.3 m. The maximum depth of 1166 m occurred in the winter of 1990 at (11N, 48W), while the minimum depth of 714 m occurred in the winter of 1984 on the equator at 41W. At each station we compute stream function from (1) using triangular interpolation in the vertical integral. We estimate the uncertainty of stream function at each station to be 11.2 m^2/s at $\sigma_\theta = 24.5$ decreasing to 2.7 m^2/s at $\sigma_\theta = 27.3$.

There are three sources of error in the stream function calculation, (1) sampling error resulting from undersampled spatial or temporal variability, (2) reference level and errors associated with the hydrostatic or geostrophic approximations, and (3) measurement error introduced by inaccuracy in the CTD and associated algorithms. We estimate the horizontal and temporal sampling error based on analysis of neighboring stations to be 15% of the stream function variability in fall and 23% of the stream function variability in spring. These sampling-based stream function error estimates give us error estimates on transport of, for example, 23.1 ± 3.5 Sv for the NECC for the fall of 1984, and 12.2 ± 2.8 Sv for the NEUC in the spring of 1989 at 44W.

The issue of reference level error, a classic problem in ocean circulation studies, has been examined by Friedrichs and Hall (1993). They find a preferred reference depth of 2100 m. We examine the error introduced by our choice of the $\sigma_\theta = 27.6$ surface using data from WESTRAX at 44W. This examination suggests a maximum error of 19%. We have varied the reference level from 800 to 2500 meters and calculated mass transport in the upper 800 m layer. The relative error of this calculations is 19% of the stream function

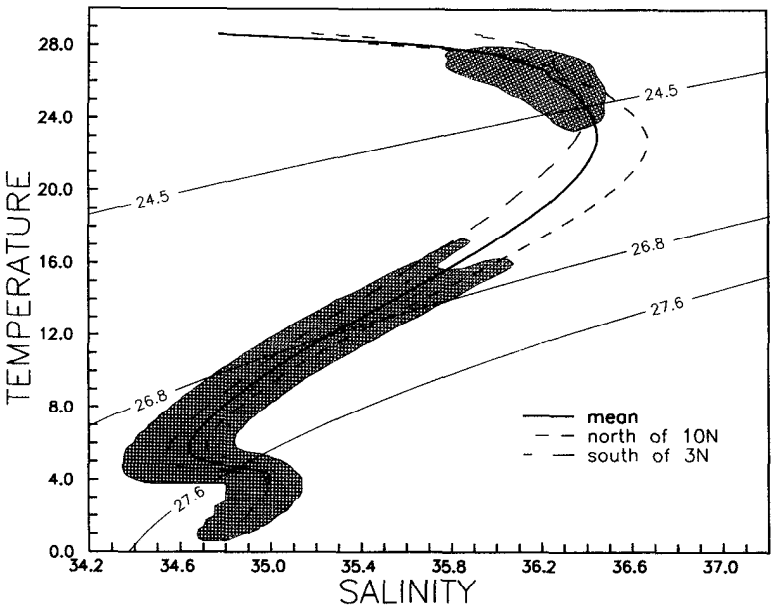

Figure 5. Temperature versus salinity in the northwest tropical Atlantic (2S–16N and 60W–35W). Shading indicates regions where more than 100 samples fall into each 0.5° × 0.05 psu bin. Bold dashed line indicates the mean relationship averaged over all profiles in the western basin. Dashed lines indicate the average for all southern stations (south of 3N) and northern stations (north of 10N). Contours of constant density are also shown. The pycnocline and intermediate water masses are bounded by the $\sigma_\theta = 24.5$, $\sigma_\theta = 26.8$, and $\sigma_\theta = 27.6$ density surfaces.

variance. The most important part of the measurement error is the systematic error due to salinity calibration problems. This only introduces a 5% relative error. The total error in upper ocean stream function, obtained by adding the individual errors (assuming independence), comes to ≈33%.

Temperature, salinity, potential density, and stream function are divided by seasons and objectively mapped onto a regular 1° × 1° grid. Each seasonal map is based on data collected typically over a 1–2 month time span. Initially we attempted to use an iterative mapping technique similar to that chosen by Levitus *et al.* (1994). However, the results were unsatisfying and were redone using statistical objective analysis (Gandin, 1963). Statistical objective analysis requires estimates of the observation error and its spatial correlation. For simplicity and consistency with previous studies we assume an isotropic Gaussian correlation function with a radius of 350 km.

As discussed in the Introduction, and as evident in the temperature-salinity census in Figure 5, three water mass types commingle in the western tropical Atlantic above 1200 m. The near surface layer reflects surface processes such as river discharge and rainfall that lead to reduced salinities. The base of this layer (and the tops of the pycnocline and thermocline) is marked by a broad salinity maximum with temperature in the range

21°–26°C and density between σ_θ = 23.8–25.3. Here we choose σ_θ = 24.5 to define this interface, following Wilson *et al.* (1994). Below the pycnocline lies cold, fresh AAIW. We choose σ_θ = 26.8 to define this interface, again consistent with Wilson *et al.* The layer between these surfaces defines the pycnocline, as well as the thermocline with which it is virtually coincident. Notice that the histogram of observations is bimodal within the pycnocline. The average northern water is 0.3 psu saltier than the average southern water for the same density. The salinity minimum near σ_θ = 27.3 identifies the signature of AAIW. We take the lower bound of this intermediate water to be σ_θ = 27.6. For comparison, Roemmich (1983) chooses σ_θ = 27.4 while Bub (1993) chooses σ_θ = 27.65. The analysis described here is limited to considering the circulation in the three layers defined by these surfaces.

3. Vertical structure with latitude

Here we examine water properties along two heavily sampled meridional sections, one at 44W representing the western basin and one at 23W representing the central basin. At 44W there were 21 hydrographic sections from 2N to at least 9N, each with better than 1° meridional resolution. Of the 21 sections three sections occurred during summer 1985, and two sections during each of fall 1984, spring 1985, spring 1989, and winter 1990. We have combined all 21 sections into 15 individual seasonal averages. To show the position of the water masses relative to the strong zonal currents, Figure 6 displays isolines of salinity and the depths of the three layer boundaries. Shading indicates the position of eastward currents. We do not attempt to estimate geostrophic currents equatorward of 2N. Salinity takes on special meaning in this discussion because, as indicated above, Southern Hemisphere thermocline water is marked by low salinities at a given density. The average of each of the four seasons is displayed in Figure 7.

We begin our discussion by examining the changes apparent in the surface layer, above σ_θ = 24.5. Within this layer there is a pronounced decrease in salinity in summer-fall to below 35 psu at depths between 0–20 m. The salinity minimum is usually located on the north side of the NECC north of 5N, which is also the location of the maximum in rainfall associated with the Intertropical Convergence Zone. However, it is important to realize that discharge from the Amazon River provides another potential source of freshwater. The latter is carried eastward by the NECC and is difficult to distinguish observationally from local rainfall. Modeling studies by Yoo and Carton (1990) suggest that both processes are important. By winter-spring the surface layer north of 5N has deepened to 100 m and its salinity has increased to greater than 36 psu. As a result, in this season the surface salinity exceeds the salinity of the upper thermocline water.

The σ_θ = 24.5 surface separates the surface and thermocline layers. At 44W this surface deepens from 95 m at the equator to 110 m at 4N and then shallows to 69 m north of 10N. Superimposed on this mean slope are substantial seasonal variations illustrated in Figure 6. It is evident that the strongest gradients of the depth of isopycnal surfaces occur in fall, associated with the intensification of the NECC.

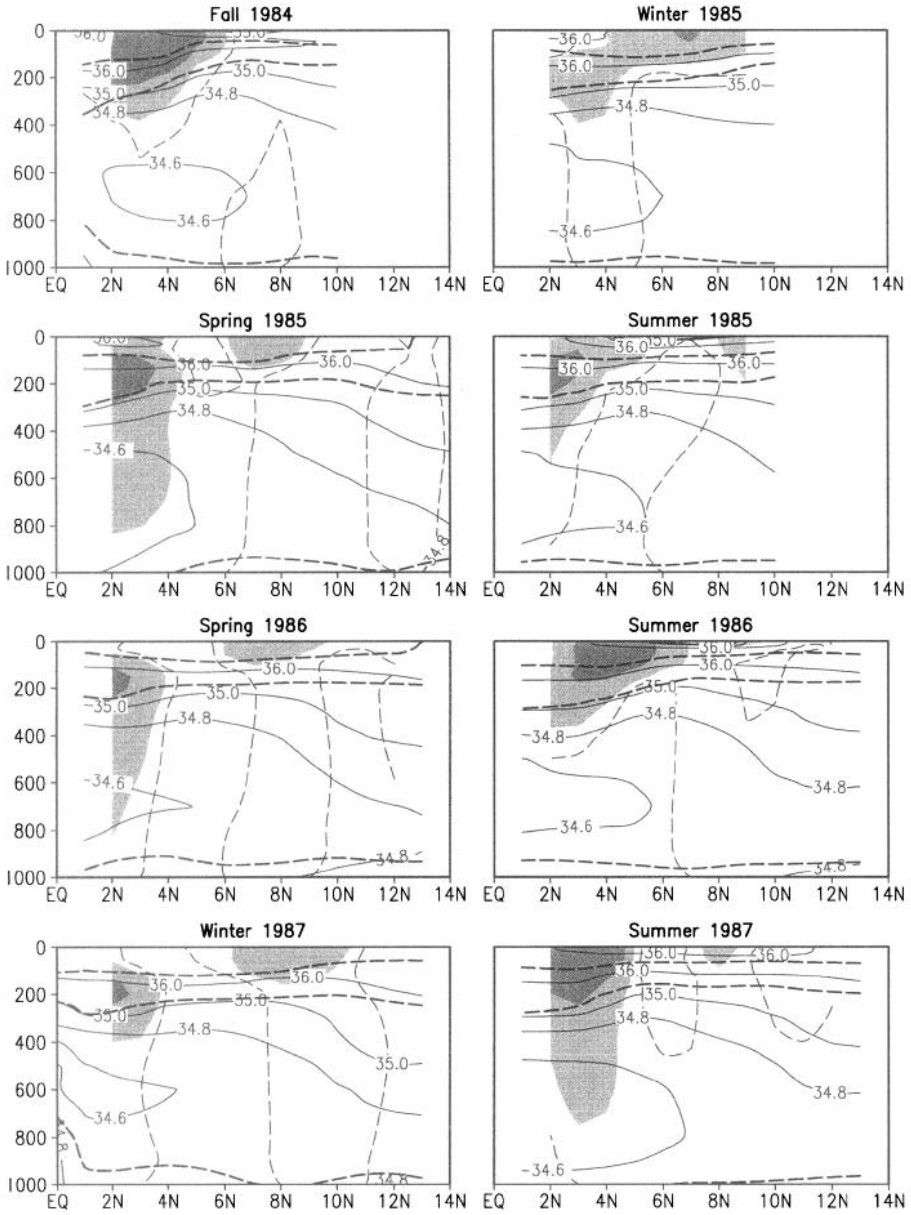

Figure 6. Depth versus latitude sections along 44W in the western basin. Salinity (thin lines) and σ_θ = 24.5, σ_θ = 26.8 and σ_θ = 27.6 (bold dash lines) are shown. Eastward zonal velocities exceeding 5 cm/sec are shaded. Zonal velocities exceeding 25 cm/sec are shaded heavily. Thin dashed line is zero zonal velocity contour.

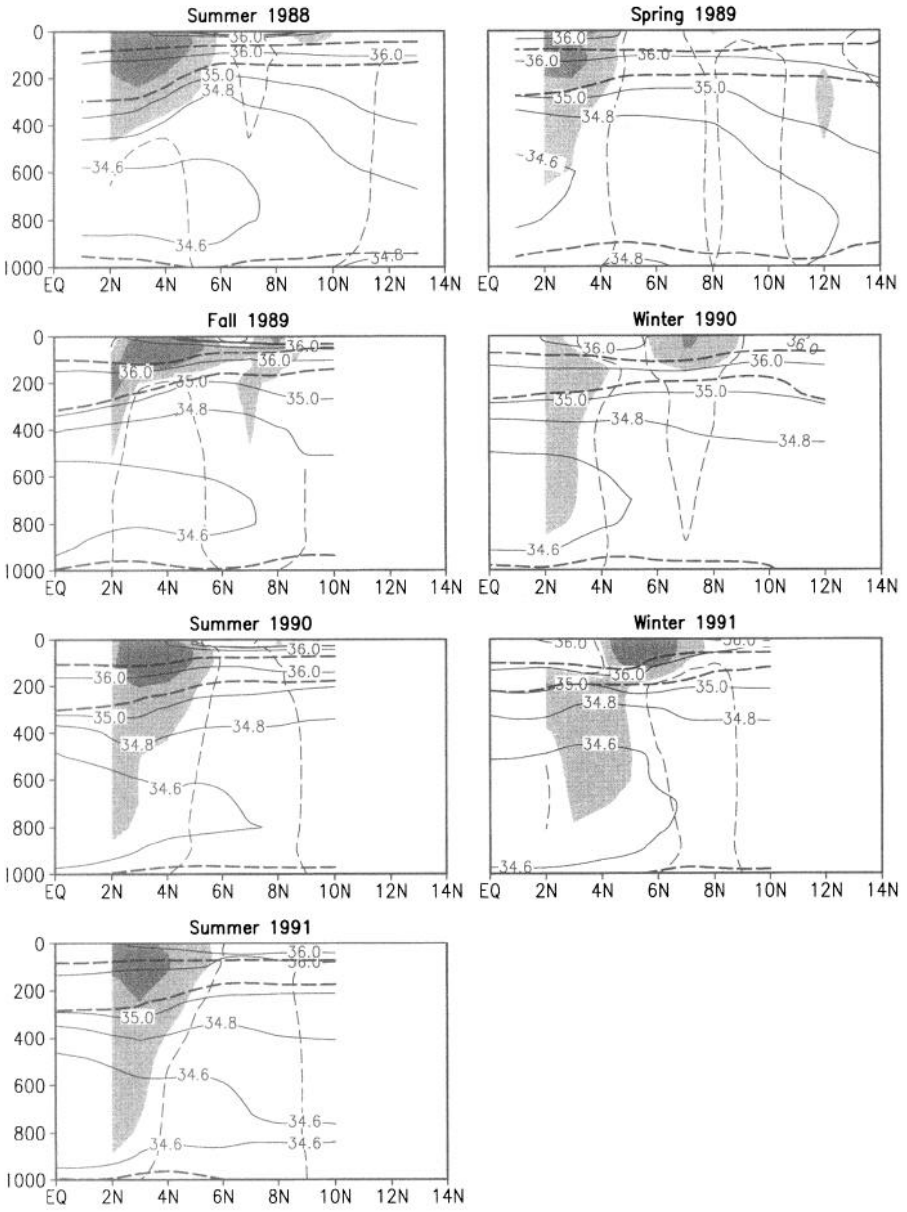

Figure 6. (Continued)

The most unusual variations of the $\sigma_\theta = 24.5$ surface at this longitude occur in the fall of 1984 and the winter of 1991. In the fall of 1984 the slope was unusually intense, with the change in depth increasing to 83 m between 3N and 7N. In the winter of 1991 the slope was also unusually strong. During this season the main change in depth occurred between 5N

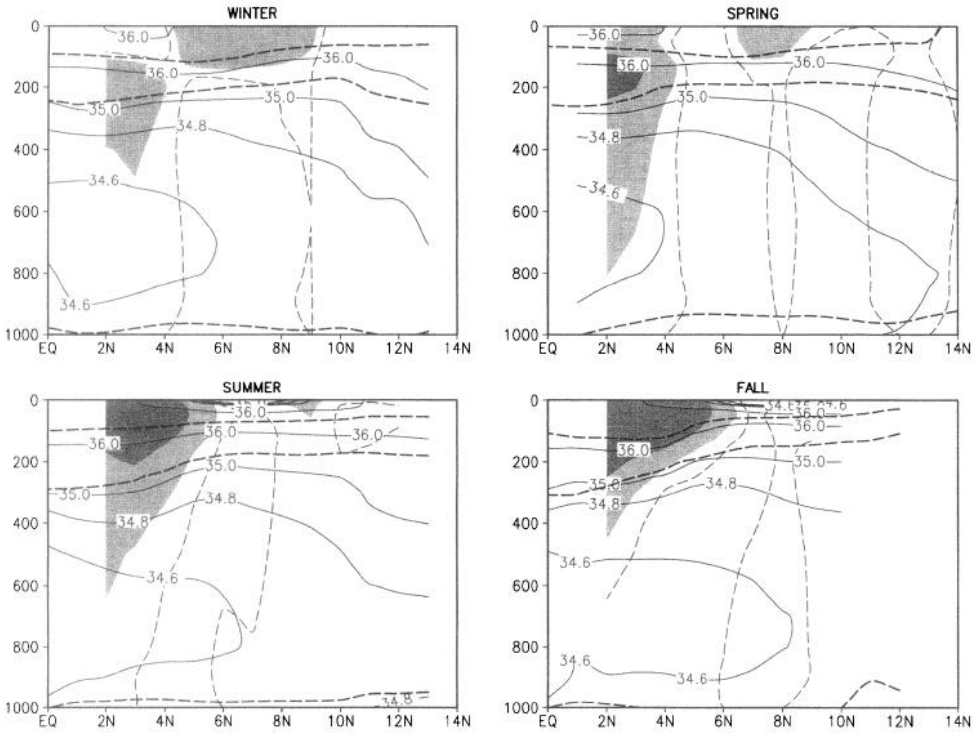

Figure 7. Climatological seasonal average salinity (thin lines) and $\sigma_\theta = 24.5$, $\sigma_\theta = 26.8$ and $\sigma_\theta = 27.6$ (bold dashed lines) plotted with depth and latitude along 44W. Eastward zonal velocities exceeding 5 cm/sec are shaded, zonal velocities exceeding 25 cm/sec are shaded heavily. Thin dashed line is zero zonal velocity contour.

and 9N and amounted to a change of 81 m. Again, this large slope implied a strong eastward current that was observed by Bub (1993) using velocity measurements.

The $\sigma_\theta = 26.8$ surface separates the thermocline and intermediate water masses. At 44W this surface has an average depth of 283 m on the equator, decreasing to 163 m at 10N, and then increasing with latitude as it enters the subtropical gyre. As with the $\sigma_\theta = 24.5$ surface, the depth of the $\sigma_\theta = 26.8$ surface changes seasonally, being deepest in fall at the equator and in spring at 10N. These seasonal changes are consistent with those documented by Molinari and Johns (1994). Interannual variations are also apparent at this depth. The strongest slope of the $\sigma_\theta = 26.8$ occurred in the fall of 1984. In contrast, the slope in the winter of 1991 was normal. This difference suggests that the anomaly in 1984 penetrated to the thermocline, but the anomaly in 1991 did not.

As suggested above, the slope of the density surfaces implies significant eastward flows that vary by season and by year. At 44W two cores of eastward current are apparent in winter and spring (Figs. 6 and 7). One of these is near surface between 7N–11N, while the other is below the thermocline south of 5N. The northern current, which can be interpreted

as the wintertime expression of the NECC, reaches an average velocity in winter of 24 cm/s and an average transport of 10.9 Sv. The maximum velocity of 34 cm/s occurred in 1991 when the transport reached 18 Sv. As summer approaches, this current gradually disappears (see, e.g., Figs. 6 and 7). The near-equatorial NEUC has an average velocity of 22 cm/s in winter. This speed increases in strength during spring to a core maximum of 35 cm/s and extends to a depth of 800 m. The maximum speed associated with this current, 43 cm/s, was recorded in spring, 1985. Geostrophic transport at 44W by the NEUC between 2N and its northern boundary in winter and spring varies from a minimum of 7 Sv in winter 1987 to a maximum of 22 Sv in spring 1985. It is interesting to compare these results with the original estimates of NEUC transport by Cochrane *et al.* (1979). Cochrane *et al.* had three pairs of stations during February–April, 1968, all west of 40W. From these pairs they estimated an eastward transport of 9 Sv. For the July–September period Cochrane *et al.* had data from several years. From this data they deduced an average transport of 28 Sv.

The seasonal vertical structure of the NECC at 44W is shown in Figure 7. Toward summer the northern countercurrent that we had previously identified as the NECC, decays. At the same time the southern NEUC raises to the surface and becomes identified in and above the thermocline as the NECC. Its disappearance from the north and reappearance in the south is the mechanism by which the NECC shifts southward in spring. Throughout the rest of the year the NECC gradually shifts northward following the shift of the Intertropical Convergence Zone. The NECC and NEUC are indistinguishable during summer and fall. The current clearly penetrates through the thermocline, extending to 400–600 m in summer and fall. This result is consistent with the current meter measurements of Richardson and Reverdin (1987) and with Doppler current profiler observations reported in Wilson *et al.* (1994). The latter set of observations shows a distinct southward shift of the core of the current with depth also evident in Figure 7.

The eastward geostrophic velocity during summer and fall is 54 cm/s, somewhat faster than the three-summer average of 45 cm/s observed in current meter measurements by Richardson and Reverdin (1987). The maximum speed of the NECC observed in our sections, 128 cm/s, occurred in the fall of 1984. These high velocities were also apparent in direct current measurements reported by Henin and Hisard (1987) in the central basin. At the time that their study was published it was speculated that the anomalous intensification of the NECC was responsible for anomalous transport of warm water into the Gulf of Guinea. The more likely explanation for the anomalous warming of the Gulf of Guinea during that year was an eastward shift of warm water along the equator (Carton and Huang, 1994). That eastward shift would have caused the intensification of the NECC as well as warming the Gulf of Guinea.

The discussion above has focussed on the changes observed in the western basin. To illustrate the changes observed in the central basin we examine water properties at 23W (Fig. 8). This longitude was discussed previously by several authors (Henin and Hisard, 1987; Garzoli and Richardson, 1989; Tsuchiya *et al.,* 1992). Here we have examined seven

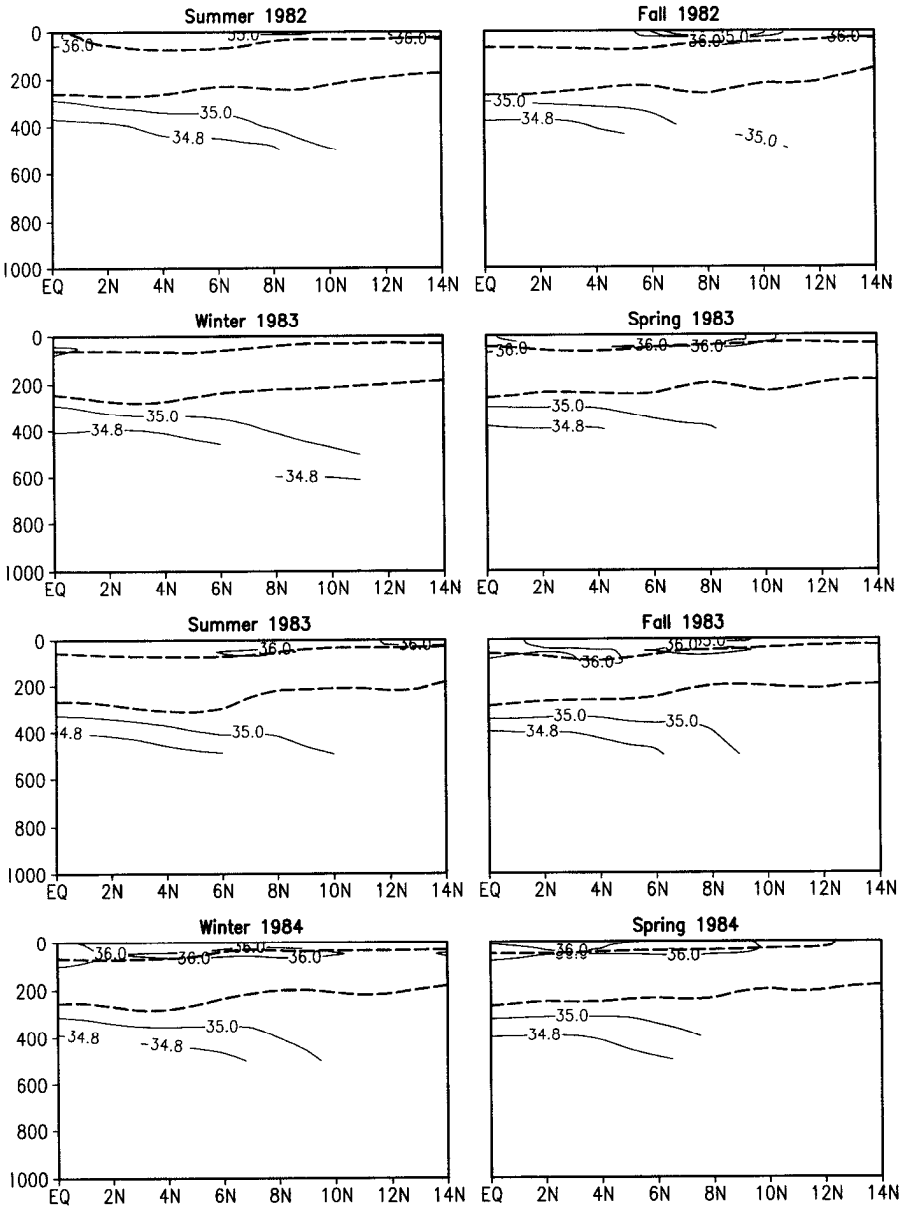

Figure 8. Similar to Figure 6 but at 23W. Salinity is uncorrected in summer 1987.

additional sections and have computed geostrophic velocities relative to the $\sigma_\theta = 27.6$ surface. No attempt has been made to present climatological seasonal averages. Fortunately as indicated by Merle (1983), seasonal variations at this longitude are less than half those farther west. The average depth of the $\sigma_\theta = 24.5$ surface is 57 ± 12 m at the equator

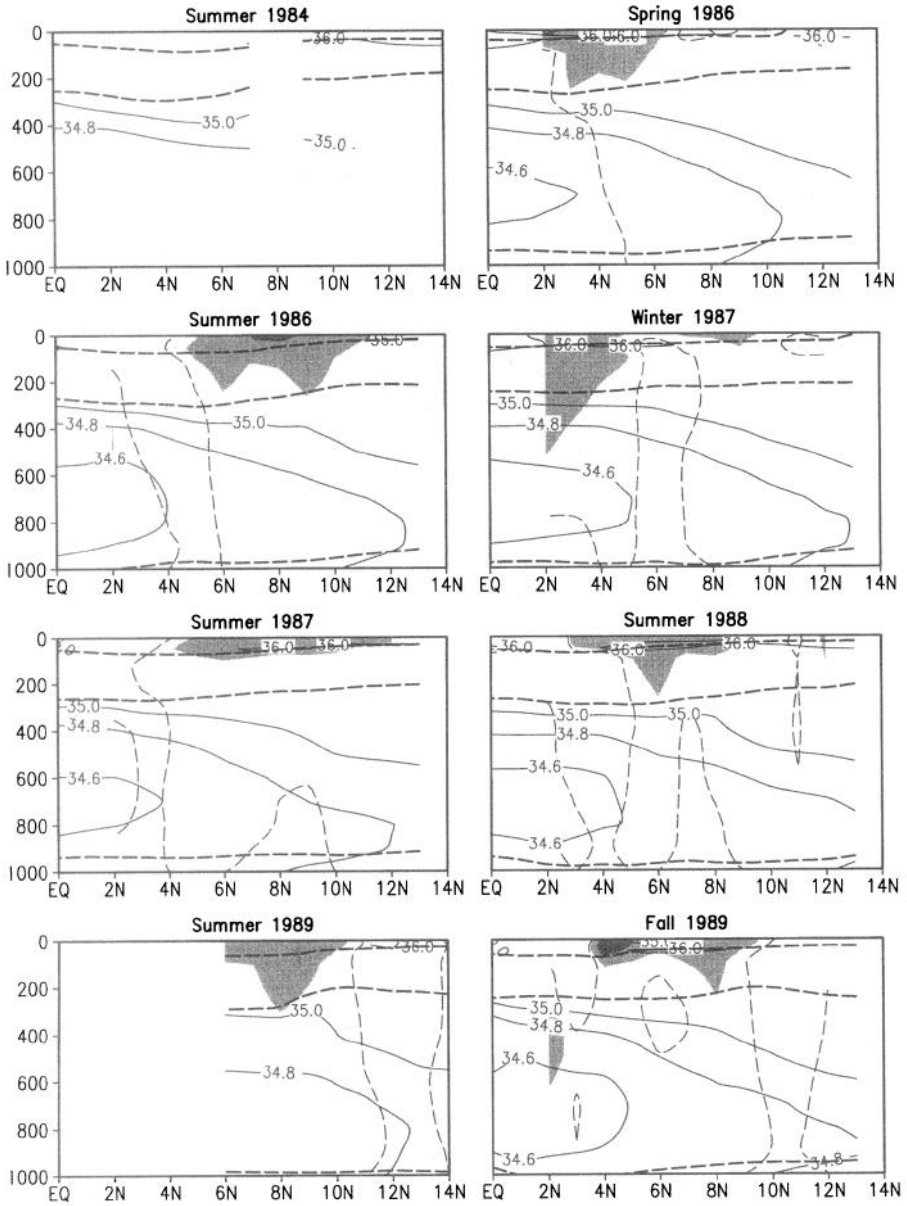

Figure 8. (Continued)

and 34 ± 4 m at 11N. The average depth of the $\sigma_\theta = 26.8$ surface is 262 ± 10 m at the equator and 214 ± 9 m at the 11N.

At 23W the NECC varies in latitude between 2N in spring to 8N in summer following the shift in the trade winds. The maximum velocity is a surprisingly stable 26 cm/s. The

only significant anomaly occurred in fall 1989 when the maximum velocity increased to 44 cm/s. The volume transport by the NECC ranges more broadly from a low of 6 Sv in the summer of 1987 to a high of 13 Sv in the summer of 1986.

4. Analysis on density surfaces

a. $\sigma_\theta = 24.5$ *surface.* As discussed above, the $\sigma_\theta = 24.5$ surface is the boundary between the surface and thermocline water masses. The $\sigma_\theta = 24.5$ surface represents most of the properties of surface water masses, except surface salinity. The height of the $\sigma_\theta = 24.5$ surface is shown in Figure 9 for each of 15 seasonal analyses in the western basin, with the corresponding geostrophic stream function shown in Figure 10. Maps of height and stream function for the four full-basin surveys are shown in Figures 11 and 12. The stream function on this surface is similar to stream function at the ocean surface.

The most prominent feature of the $\sigma_\theta = 24.5$ surface is the NECC ridge/trough system. This system is most pronounced in summer when it extends continuously from west to east between 3N and 10N. The basinwide surveys show that between 35W and 30W the NECC divides into two flows, one (12 Sv in the summer of 1986 and 9 Sv in the summer of 1987) turning southward and the other (13 Sv in the summer of 1986 and 6 Sv in the summer of 1987) continuing eastward. During the fall of 1984 the meridional gradient between the NECC trough and ridge was especially intense. In this season the $\sigma_\theta = 24.5$ surface rose more than 95 m between 3N and 7N.

The summer of 1987 had the most impressive meandering between 42W and 35W. This meander was due to the presence of a large cyclonic eddy between 5N and 12N. The eddy extended throughout the upper layers of the water column. Independent confirmation for the existence of this eddy is provided by the inverted echo sounder time series of Katz (1993). At 38W Katz reported a drop of dynamic height of more than 12 dyn. cm at 9N. We have examined the temperature-salinity characteristics of this eddy and found them to resemble the surrounding water closely. We conclude from this that the cyclonic feature resulted from an uplift of the thermocline rather than horizontal advection of anomalous water.

b. $\sigma_\theta = 26.0$ *surface.* The $\sigma_\theta = 26.0$ surface is representative of the thermocline. The depth of the $\sigma_\theta = 26.8$ surface indicates the base of the thermocline. The stream function in the thermocline is shown in Figures 13 and 14 for the western basin. Shading has been added to Figure 14 to show low salinity (<35.6 psu) southern water as it intrudes into the Northern Hemisphere along this isopycnal surface. The corresponding depth and stream function maps for the basinwide surveys are shown in Figures 15 and 16. Shading hasn't been added to these because mixing is sufficiently large in the central and eastern basin to prevent identification of southern water.

As indicated in Section 3 horizontal currents at the depth of the middle of the thermocline are rather different from currents within the mixed layer and upper thermo-

cline (compare Figs. 12 and 16). The NEUC is present during all seasons to the east of 40W. The average transport north of 2N is 17 Sv. However, to the east of the 35W the NEUC loses water to the equatorial zone (average 8 Sv), a phenomenon that was also evident in the surface layer. East of 30W the two countercurrents, the NECC and the NEUC, become increasingly difficult to separate.

The only occasion when we have sufficient data to observe the fate of water within the NECC is in the summer of 1986. During this season a total of 26 Sv was diverted northward near 21W. This leaves only 13 Sv continuing eastward. The magnitude of this northward transport is astonishing because it approaches the annual average northward warm water transport across this latitude. Part of this northward flow re-enters the North Equatorial Current north of 12N. Coincident altimeter sea level measurements from Geosat (Fig. 17a) are reassuringly consistent with stream function in the surface layer, but quite different from the stream function at the base of the thermocline. Much of the northward movement of southern water occurs in the western basin. In this region we can use the salinity difference between southern and northern waters to track this water. It is striking that southern water does not intrude into the Northern Hemisphere as an organized current. In summer it forms a pool south of the latitude of the NECC, but north of the NEUC. In contrast, in winter and spring southern water is confined to a smaller pool south of the NEUC. The change in volume with season of these pools is responsible for 3–5 Sv of northward transport. This value is similar in magnitude to the amount of water being transported northward in the North Brazil Current. This water is removed seasonally either by Ekman drift, as suggested by Roemmich (1983) and investigated by Reverdin *et al.* (1993), or by anticyclonic eddies, as suggested by Fratantoni *et al.* (1995).

Year-to-year variations in the pooling of southern water are large. This is especially true in winter and spring. In the winter of 1986–87 the NEUC was weak and southern water penetrated to 10N within the thermocline. In the winter of 1989–1990 the NEUC existed only eastward of 47W so west of this longitude southern water penetrated as far north as 14N. Our data set is too limited to quantify the year-to-year variations in this pooling.

c. σ_θ = 27.3 surface. Between σ_θ = 26.8 and σ_θ = 27.6 surfaces lies the AAIW. Low salinity (33.9–34.6 psu) AAIW forms in the South Atlantic subtropical gyre. The behavior of this water mass is described in Warner and Weiss (1992), Tsuchiya *et al.* (1992), and Gouriou and Reverdin (1992). Gouriou and Reverdin identify intensive interaction between AAIW and surface water in the equatorial region. They estimate that subsurface waters below σ_θ = 26.5 are entrained into the surface layer at rate of 11–12 Sv within 5° of the equator. The stream function at the core depth of this water mass (σ_θ = 27.3) is shown in Figure 18 for each of 15 seasonal analysis in the western basin and in Figure 19 for the basinwide surveys. As in Figure 14, shading has been added to show low salinity (<34.6 psu) water. The currents below the thermocline do not exceed 5 cm/sec and are quite noisy, with little seasonal variation. Salinity has a distinctly zonal structure with a

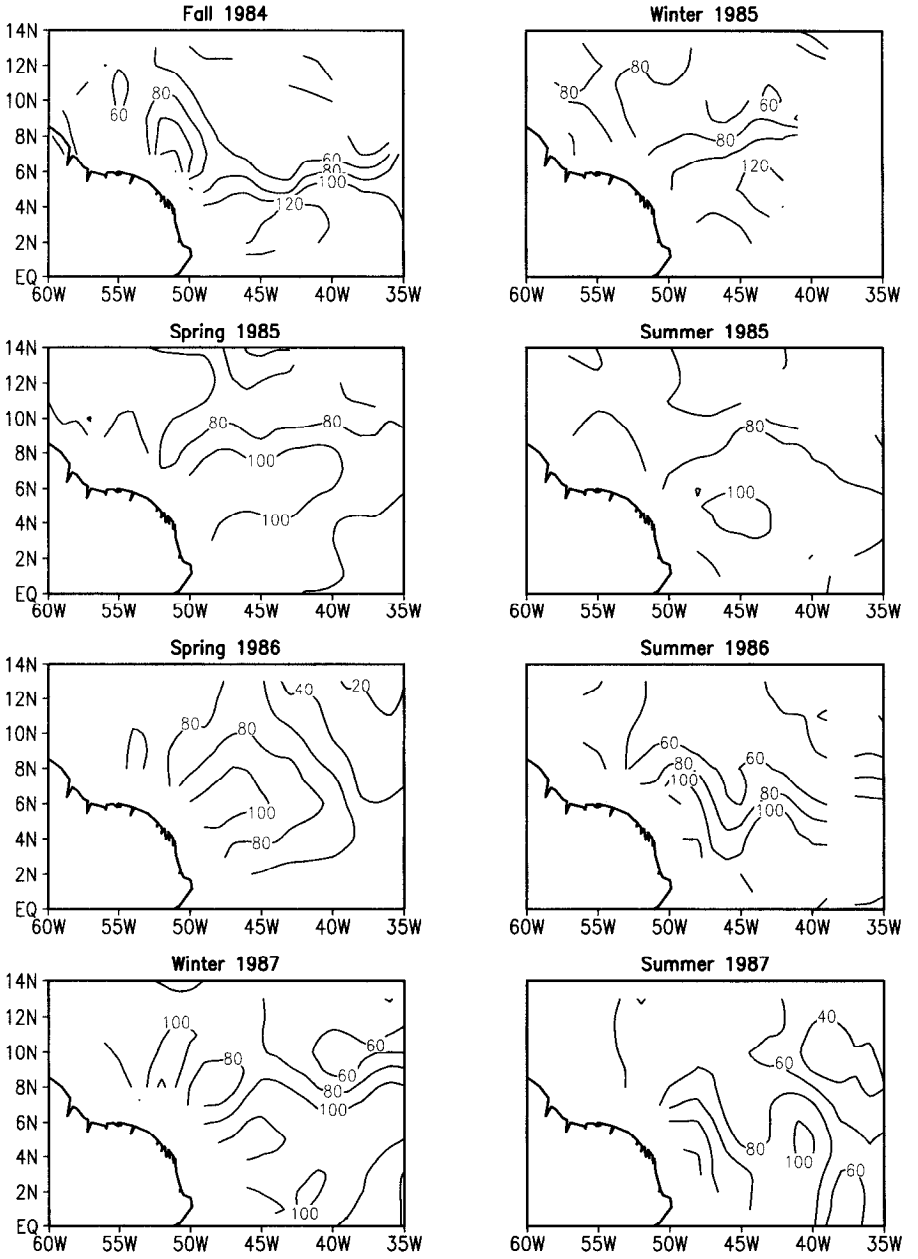

Figure 9. Pressure on the $\sigma_\theta = 24.5$ surface in the western basin. Units are db.

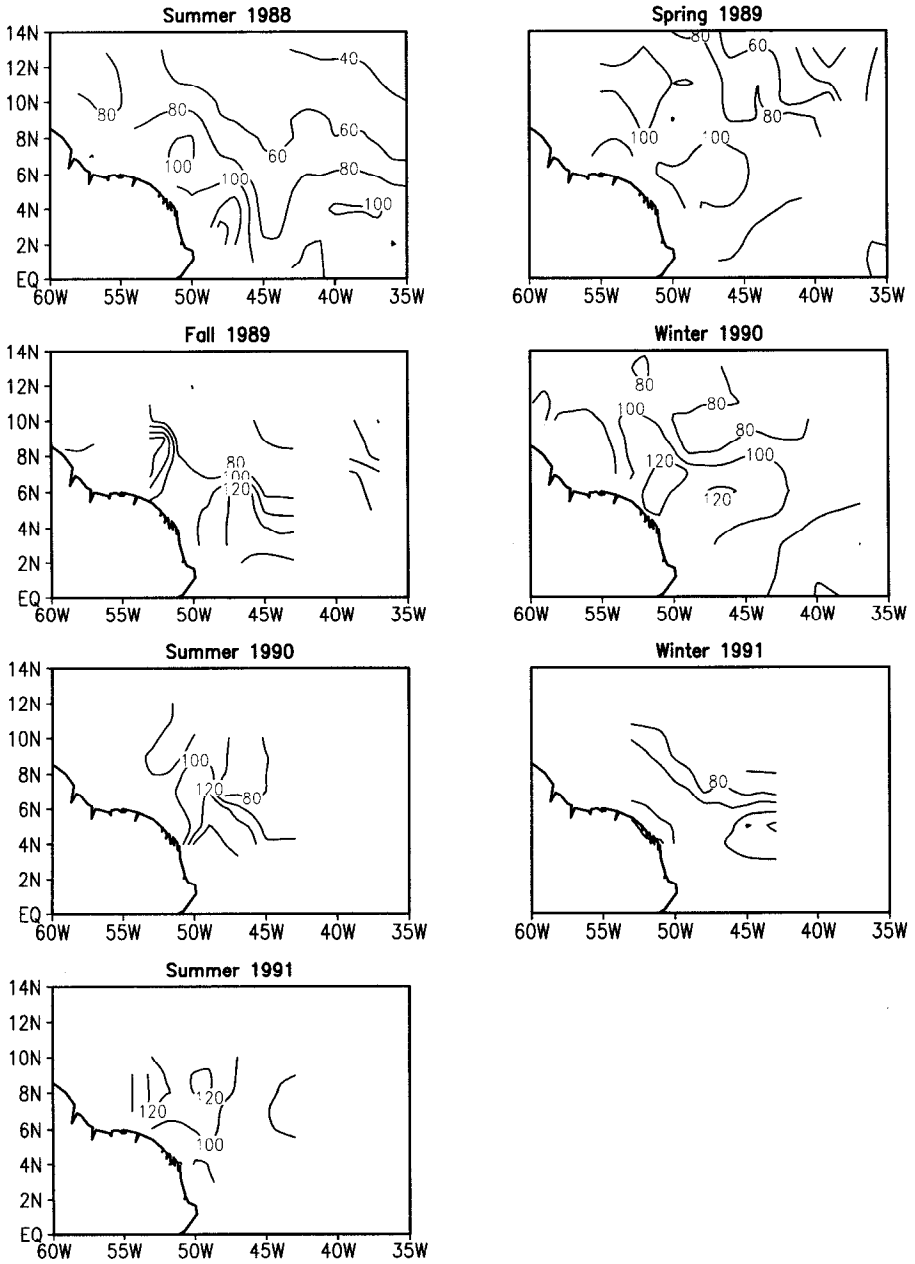

Figure 9. (Continued)

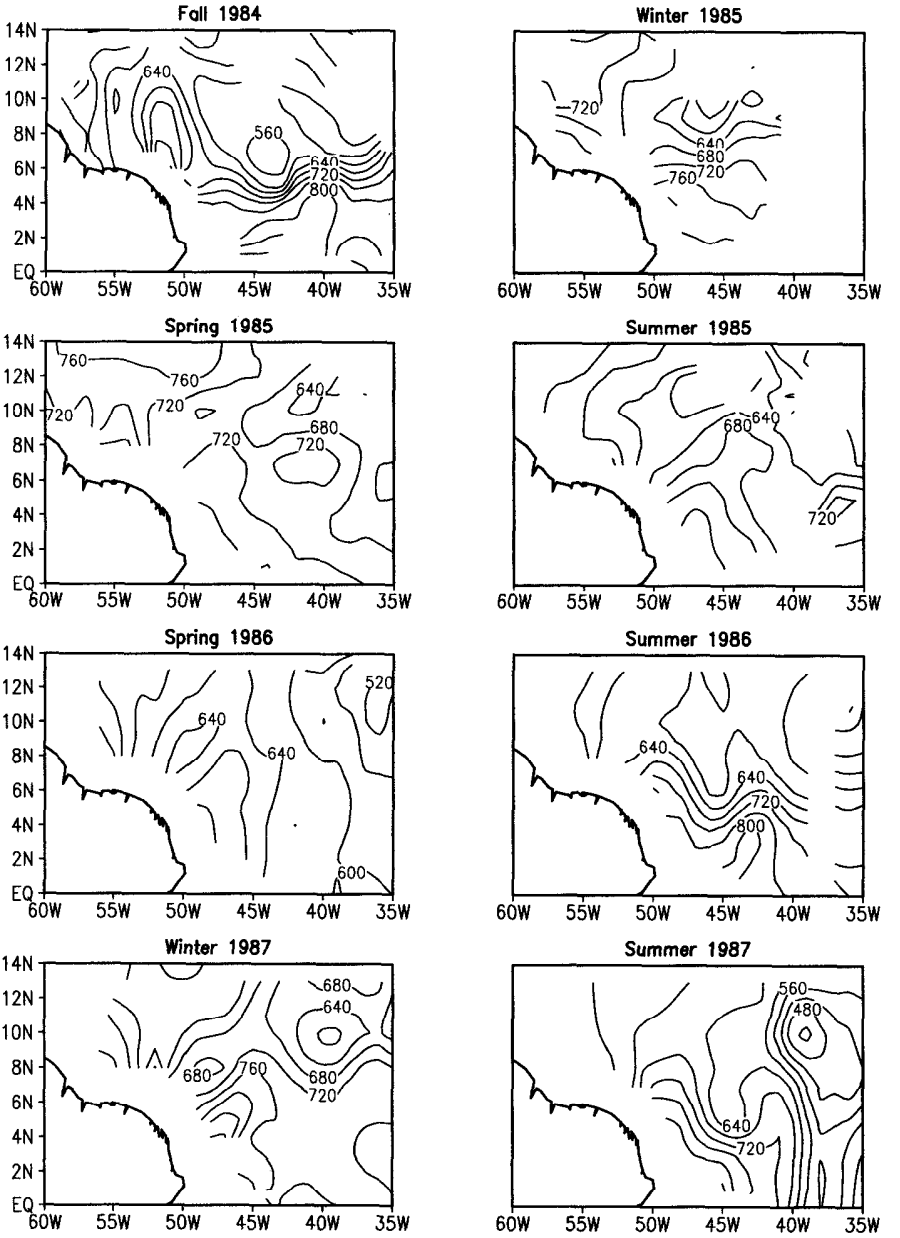

Figure 10. Stream function on the surface $\sigma_\theta = 24.5$ in the western basin. Units are 10^2 m^2/s^2.

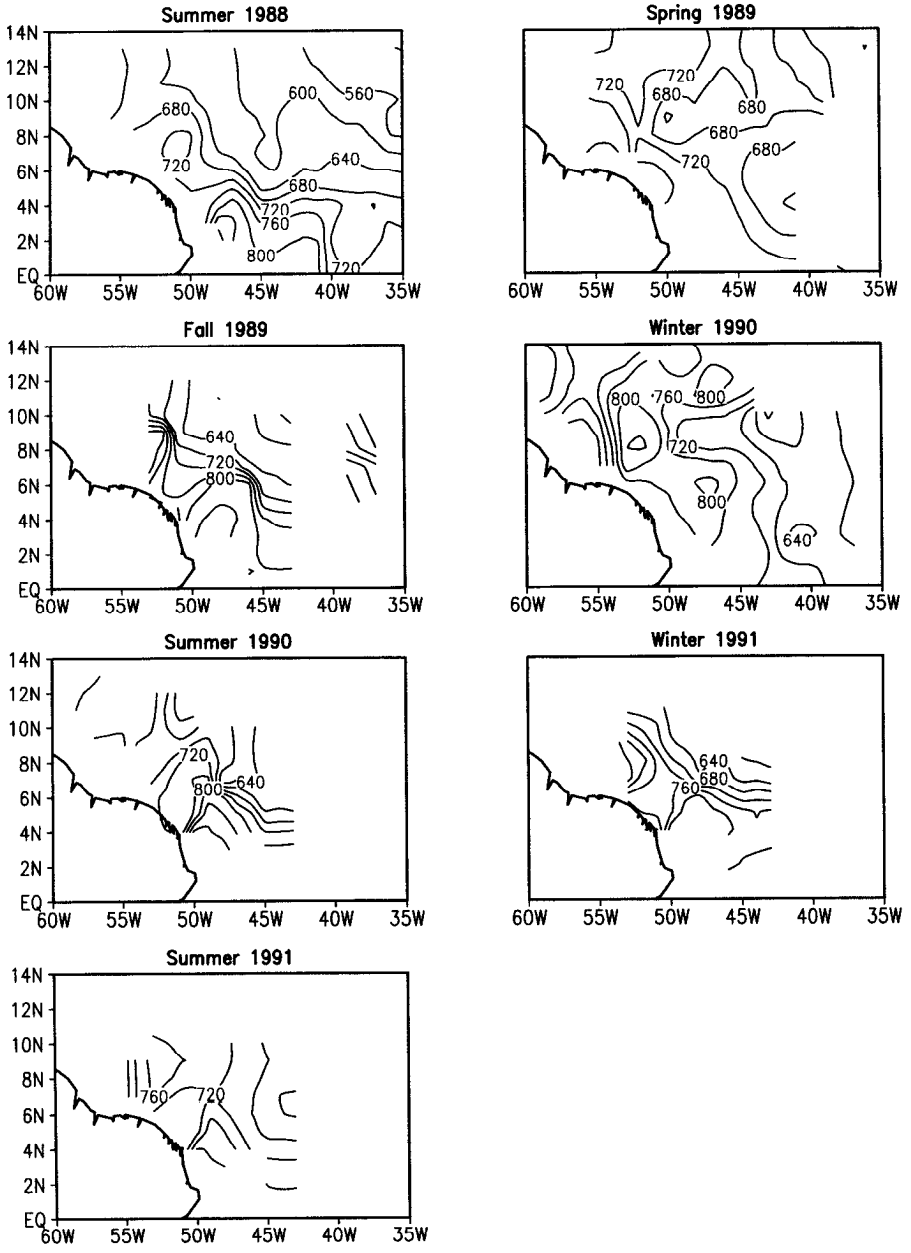

Figure 10. (Continued)

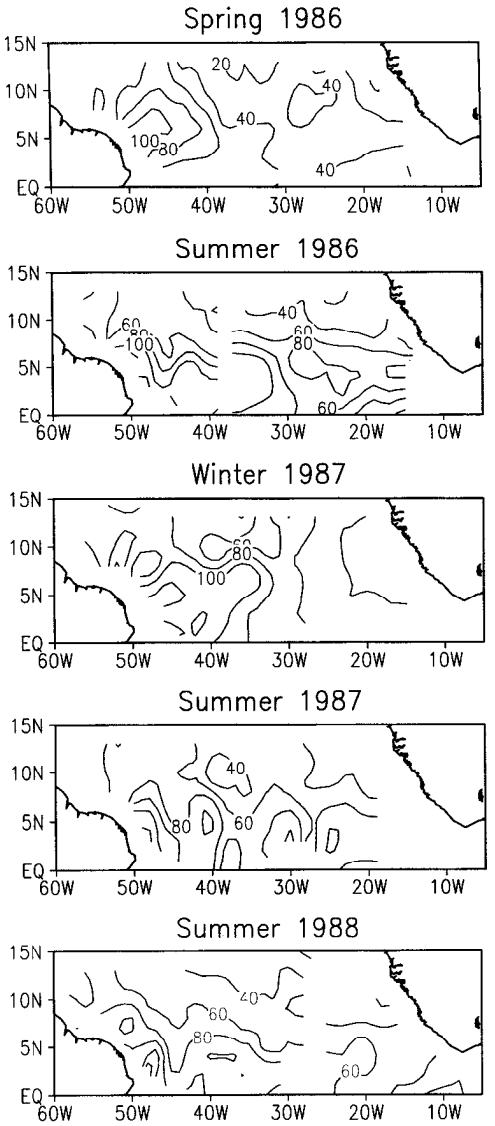

Figure 11. Pressure on the $\sigma_\theta = 24.5$ surface during the basinwide surveys. Units are db. Salinity is uncorrected east of 33W in the summer of 1987.

northward shift near South America. The basinwide surveys Figure 19 show that water in the central basin is saltier than in the west, except during the summer of 1986.

5. Summary and conclusions

The water mass properties of the upper layers of the tropical Atlantic were first examined by Defant (1936) using observations from the groundbreaking Meteor surveys of 1924 and

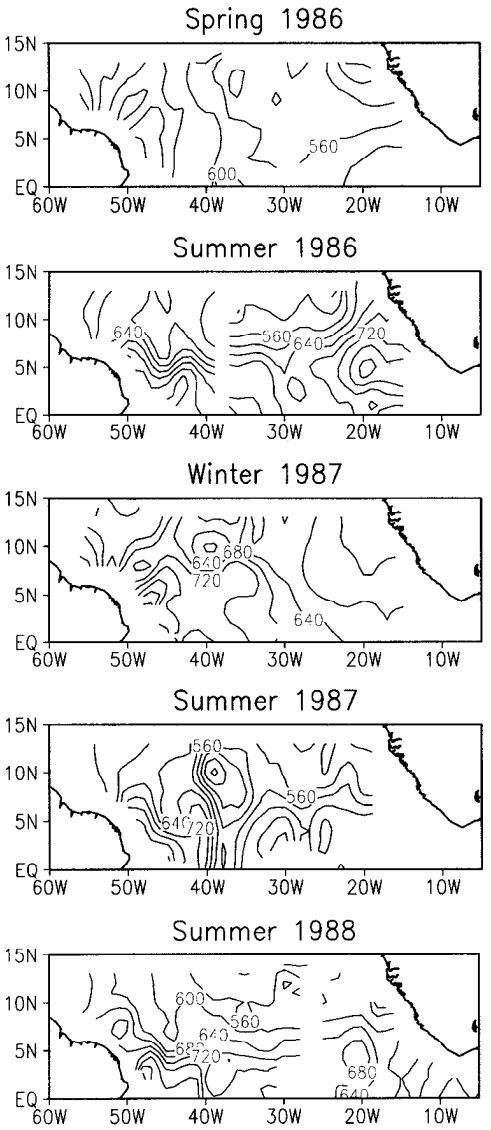

Figure 12. Stream function on the σ_θ = 24.5 surface during the basinwide surveys. Units are 10^2 m^2/s^2. Salinity is uncorrected east of 33W in the summer of 1987.

1926. The current study can be viewed as an extension of this early work and later efforts by investigators in the FOCAL, SECTIONS, and WESTRAX programs to examine synoptic, seasonal, and interannual variations. Here we present a remarkable set of hydrographic measurements covering the ten-year period 1982–1991. The data are particularly extensive in the western basin and are sufficient to allow construction of 15

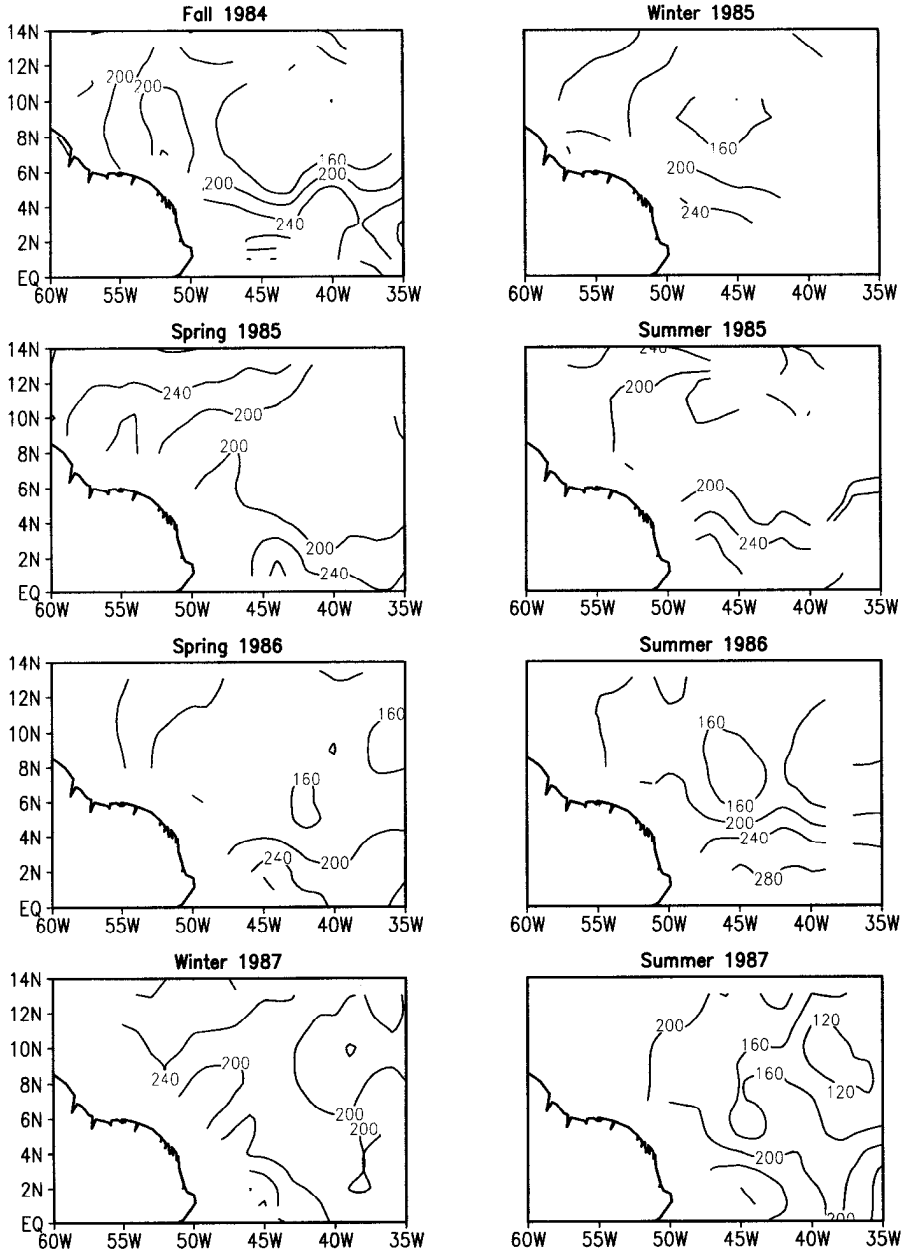

Figure 13. Similar to Figure 9 but for the $\sigma_\theta = 26.8$.

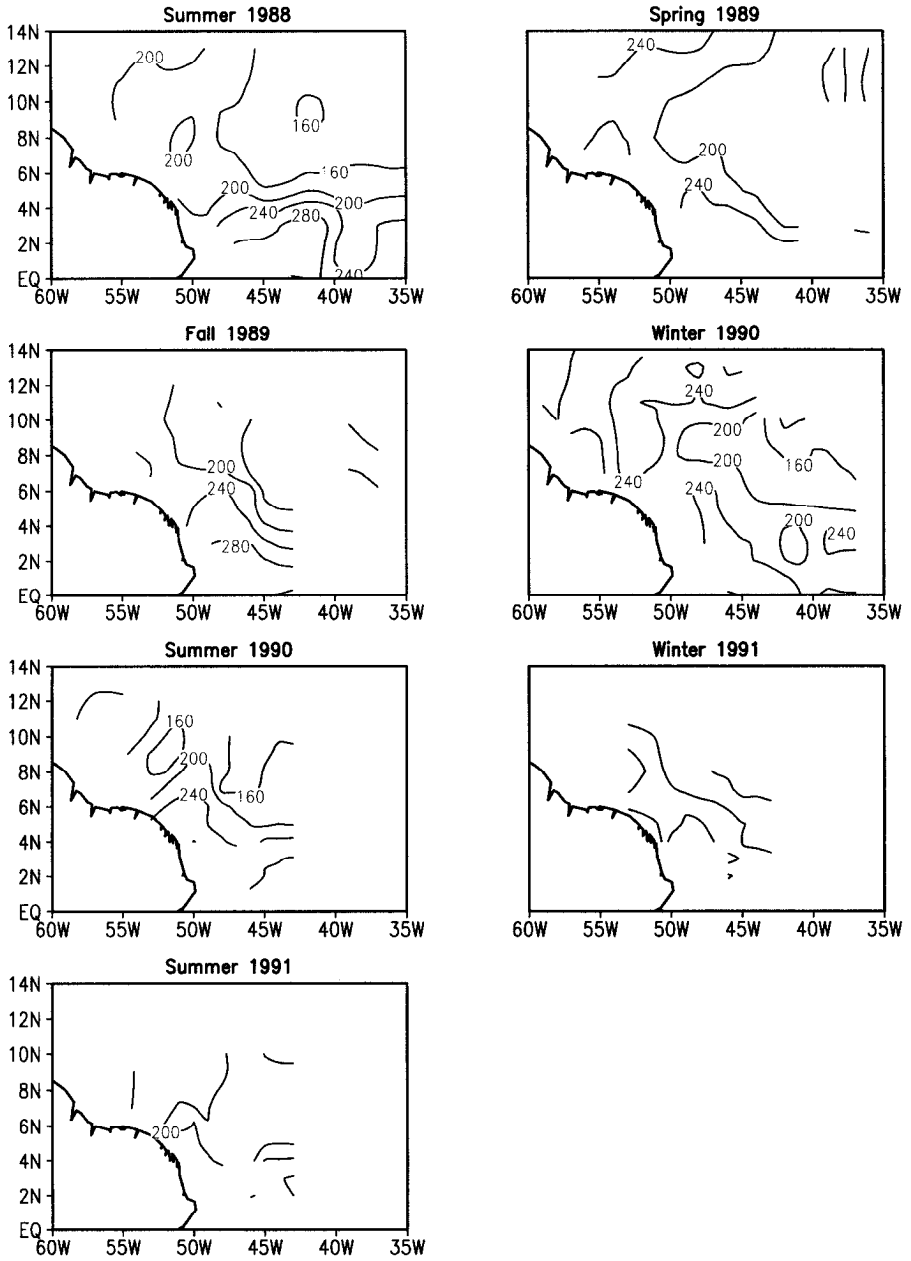

Figure 13. (Continued)

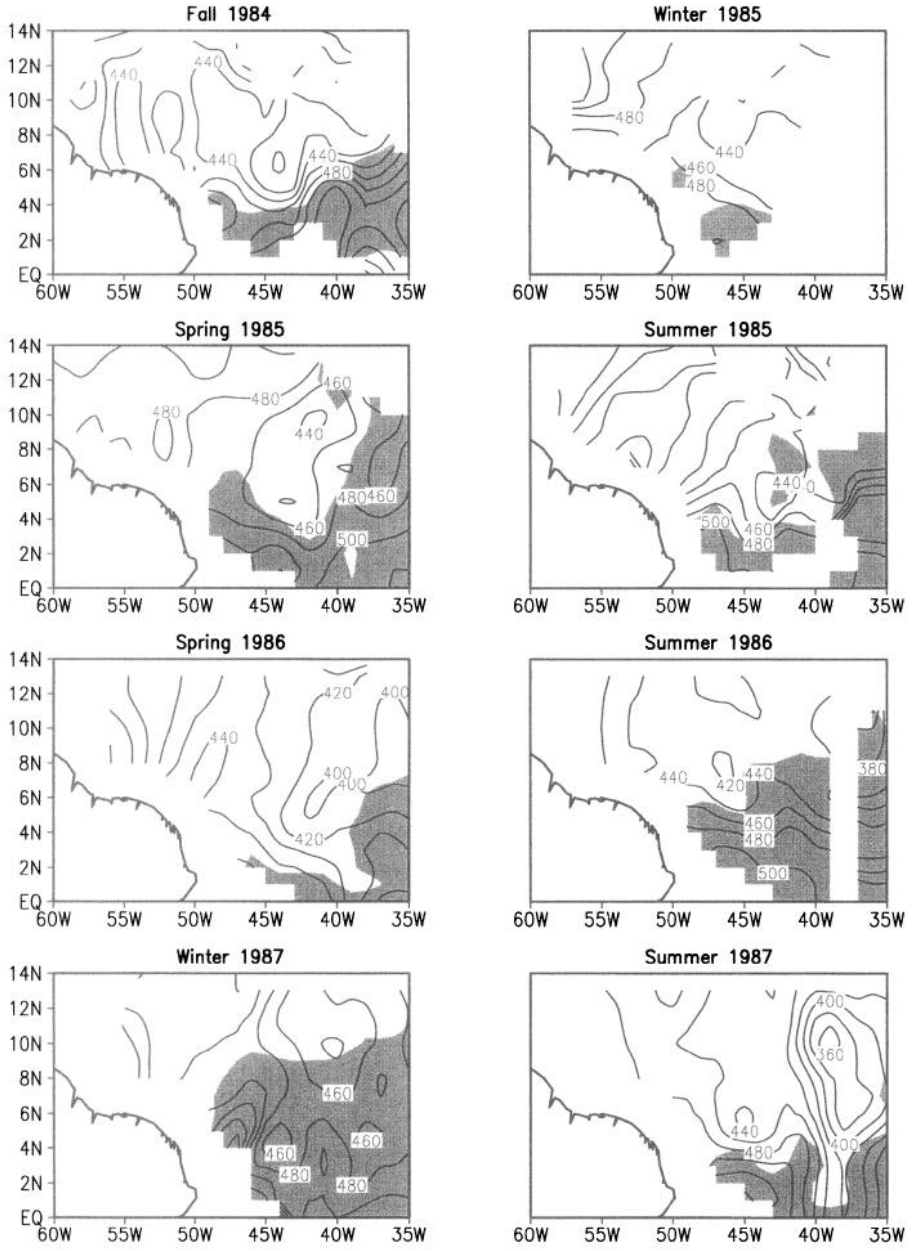

Figure 14. Stream function on the σ_θ = 26.0 surface in the western basin. Units are 10^2 m^2/s^2. Salinities below 35.6 psu on this surface are shaded.

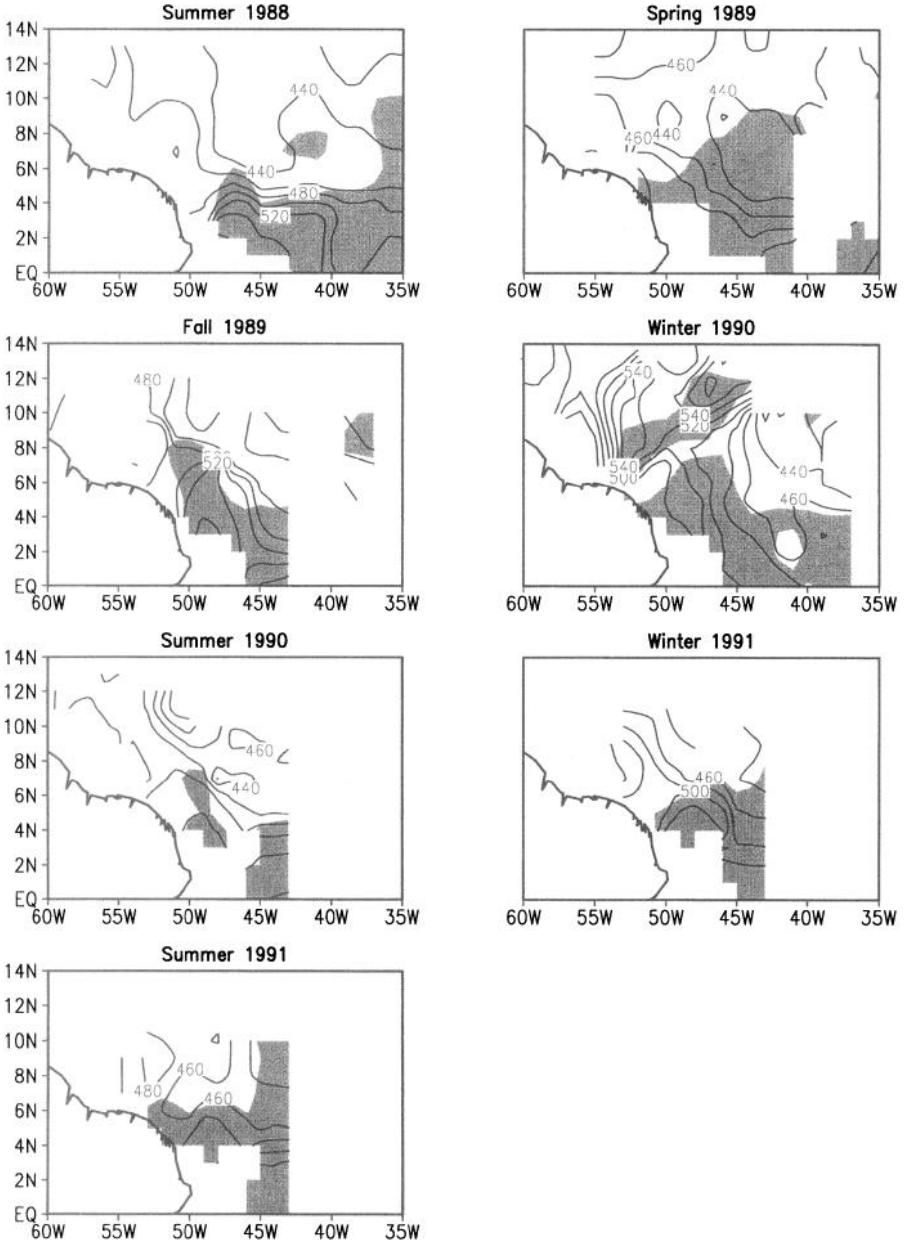

Figure 14. (Continued)

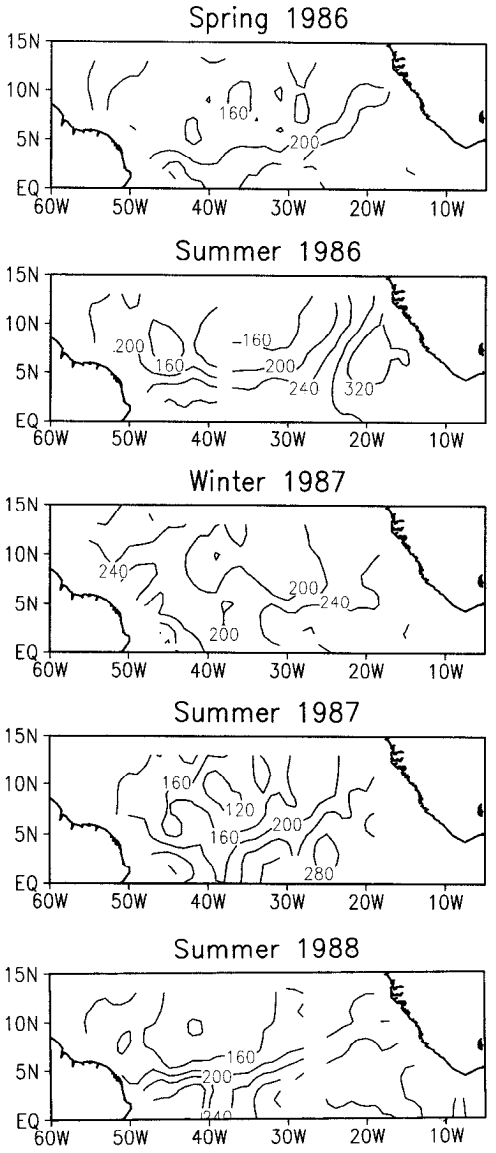

Figure 15. Similar to Figure 11 but for $\sigma_\theta = 26.8$.

seasonal temperature and salinity analyses to 1200 m depth. This depth is close to the interface between Antarctic Intermediate Water and North Atlantic Deep Water. Besides the western surveys and a few eastern surveys, five multi-ship basinwide surveys were conducted. These latter allow us to construct gridded fields for the whole northern basin representing a 2–3 month average. Together these data have irreplaceable information about changes in tropical Atlantic circulation during the 1980s. The combined data set

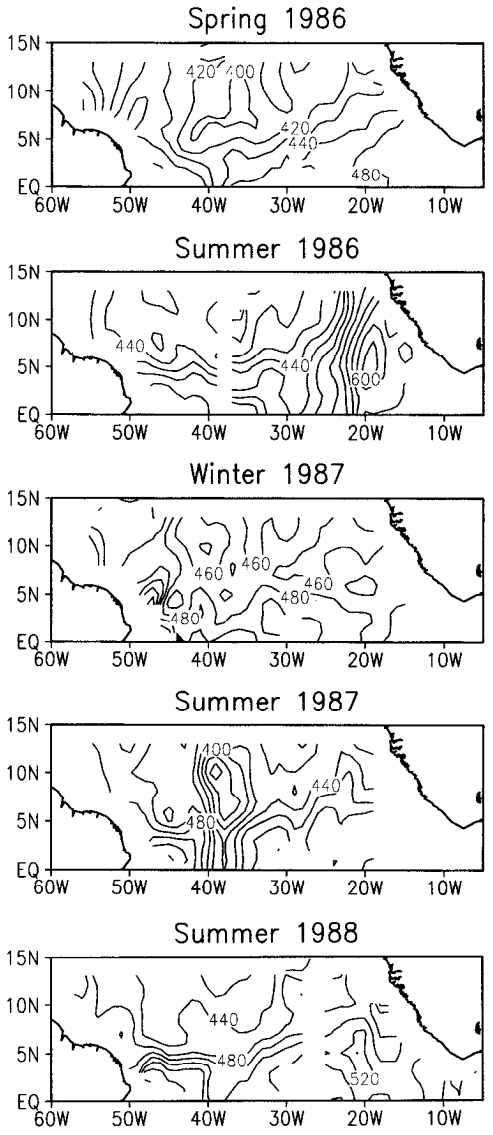

Figure 16. Similar to Figure 12 but for $\sigma_\theta = 26.0$.

provides information about the three dimensional structure of temperature, salinity, and currents, in this important ocean basin.

The analysis portion of the paper is divided into an examination of the vertical structure at a western and eastern longitude, and analysis of the horizontal structure at the top and base of the thermocline. The surface layer, containing water with densities less than σ_θ = 24.5, is generally shallower than 110 m at the equator, becoming even shallower toward the

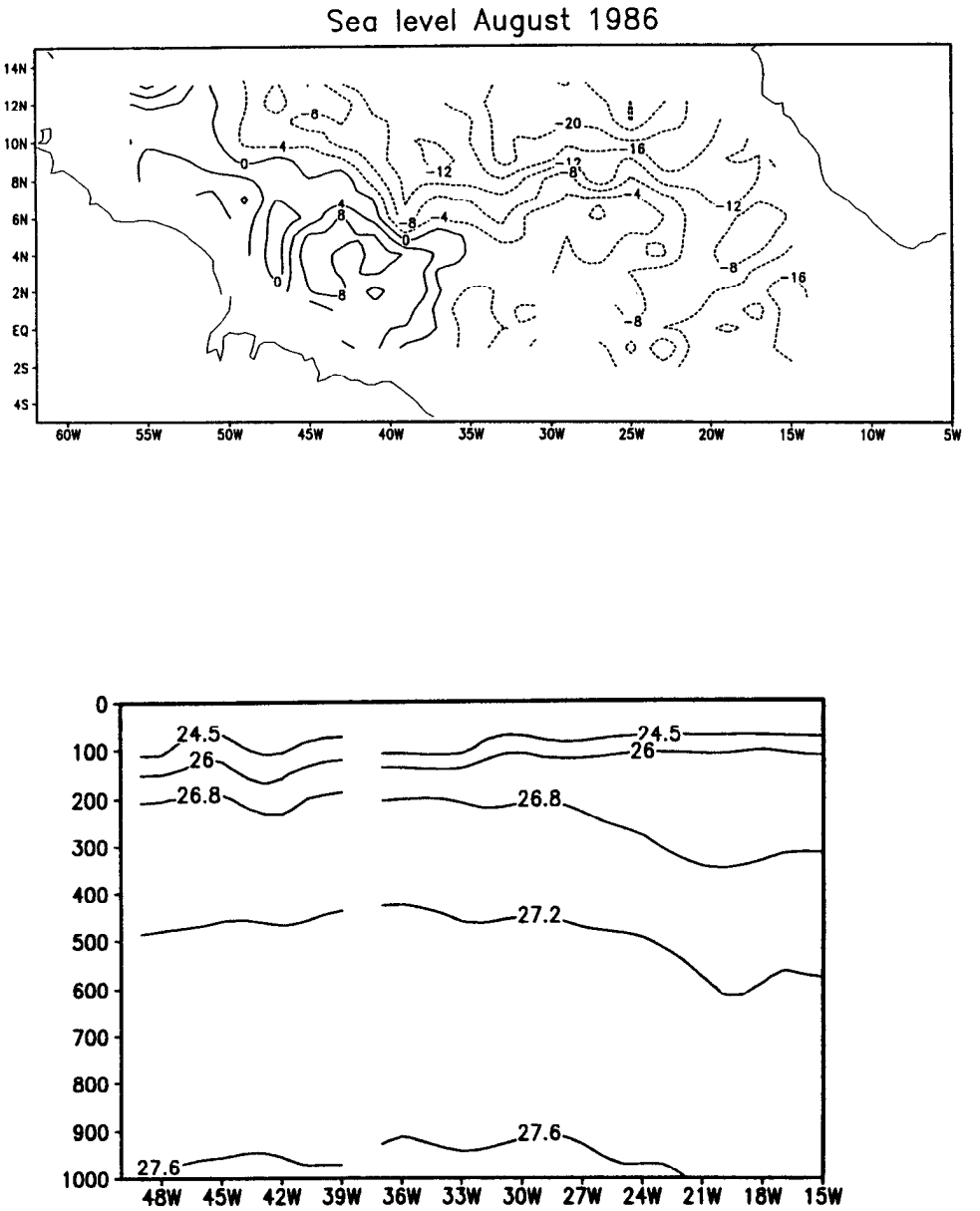

Figure 17. (a) GEOSAT sea level in August 1986. Units are cm, (b) depth versus longitude section along 5N in summer 1986. σ_θ = 27.6, 27.2, 26.8, 26.0, and 24.5 are shown.

north. At the top of this layer there is a pronounced low salinity layer in summer–fall where seasonal averages drop well below 35 psu. The surface salinity minimum is usually located on the northern side of the NECC, north of 5N. This is also the location of the band of rainfall associated with the Intertropical Convergence Zone. By winter–spring the surface layer north of 5N has deepened to 100 m. Its salinity has increased to greater than 36 psu so that the surface salinity exceeds the salinity of the upper thermocline water.

The pycnocline, which coincides with the thermocline here, spans depths between 100 m and 300 m at the equator at 44W. This is a layer of active interhemispheric transport in which southern water of lesser salinity crosses the equator. During winter and spring there are two cores of eastward flowing current. The northern of these, the NECC, is in the surface layer between 7N and 11N. It reaches an average speed of 24 cm/s at 44W, with an average seasonal transport of 10.9 Sv.

The other eastward current, the NEUC, is found in and below the thermocline south of 5N. This southern current has an average winter velocity of 22 cm/s, increasing considerably during the spring to a core average of 35 cm/s. Transport estimates for the NECC vary in the range of 7 Sv to 22 Sv. Toward summer this southern current makes its appearance at the surface, shifts northward, and becomes the NECC. The NECC in the western basin reaches an average velocity of 54 cm/s at 3–4N in summer–fall, shifting northward to 7–8N where it disappears in spring, only to reappear again in the south.

To the east of 30W the NECC bifurcates (Fig. 12). One branch turns southward, contributing its water to the equatorial current system. The other branch turns northward near the African coast. The average transport of the NECC at 23W is reduced to 8.5 Sv, but remains fairly stable throughout the year.

In the Introduction we pointed out uncertainties in our knowledge of the route by which southern water enters the northern subtropical gyre. The total average northward mass transport in the upper 1200 meters at 12N calculated from our data is 6.7 $\pm$ 1.2 Sv (Chepurin and Carton, 1997). This estimate is consistent with the 5.2 Sv estimate of Friedrichs and Hall (1993) at 11N. This northward transport is the net result of intensive interhemispheric water exchange. Of the 13 Sv of southern water believed to cross the equator and enter the subtropical gyre (Schmitz and Richardson, 1991) only 2 Sv are believed to move northward in the seasonal North Brazil Current north of the NECC. Another 3–4 Sv are believed to move northward in the anticyclonic rings generated at the confluence of the North Brazil Current and the NECC (Fratantoni *et al.*, 1995). Evidence is presented in this study that 3–5 Sv moves northward as a result of the seasonal shift of the NECC. It is possible that some of this transport occurs through eddies and rings generated at the confluence of the currents. These results still leave a relatively broad range estimates of between 2 and 8 Sv of southern water entering the subtropical gyre by transiting the North Brazil Current, entering the NECC, and exiting northwards east of 23W.

The observations presented in this study show that besides strong seasonal variations, the circulation in the upper levels of the Atlantic has substantial interannual variations. A striking example of this occurred in the summer of 1986. During this summer a remarkable

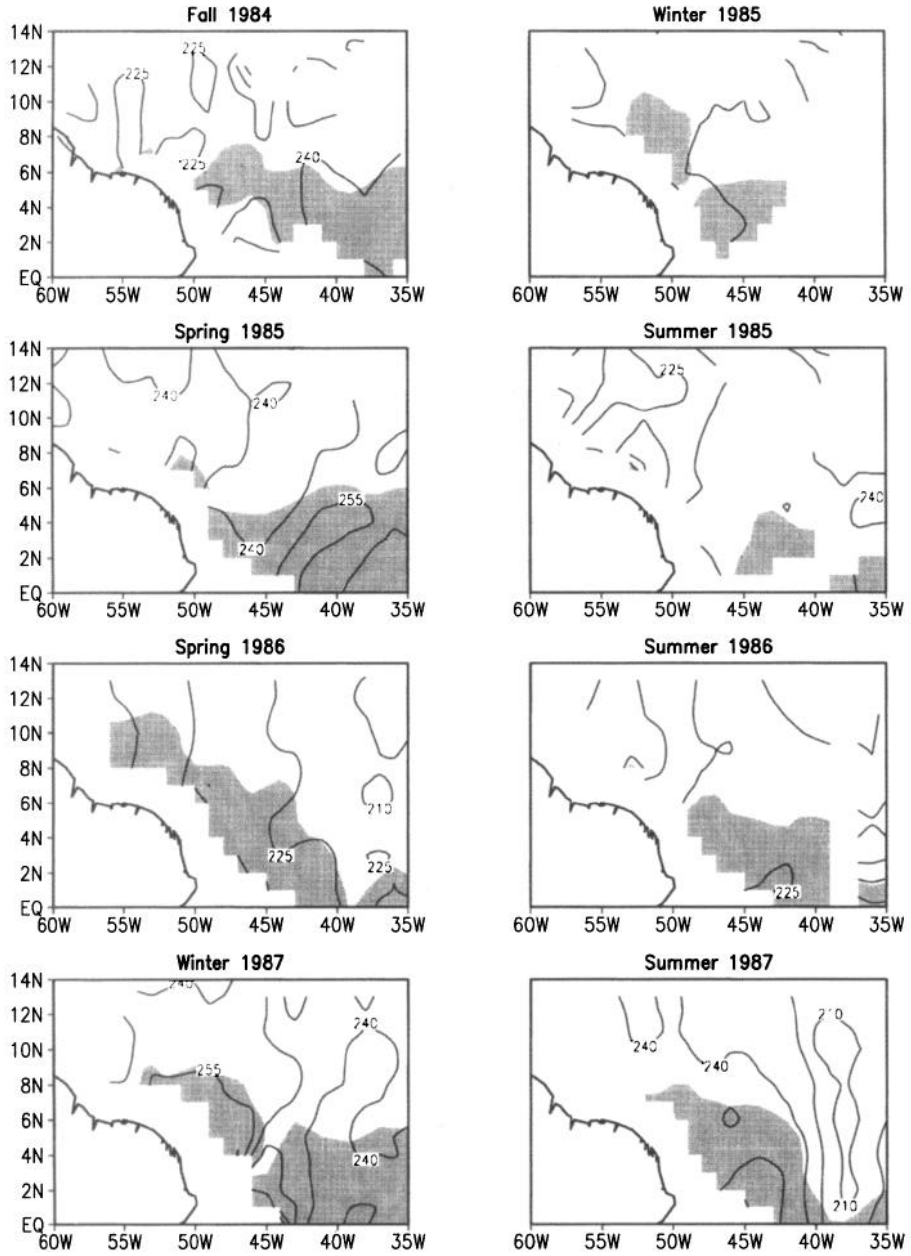

Figure 18. Stream function on the $\sigma_\theta = 27.3$ surface in the western basin. Units are $10^2 \cdot m^2/s^2$. Salinities below 34.6 psu on this surface are shaded.

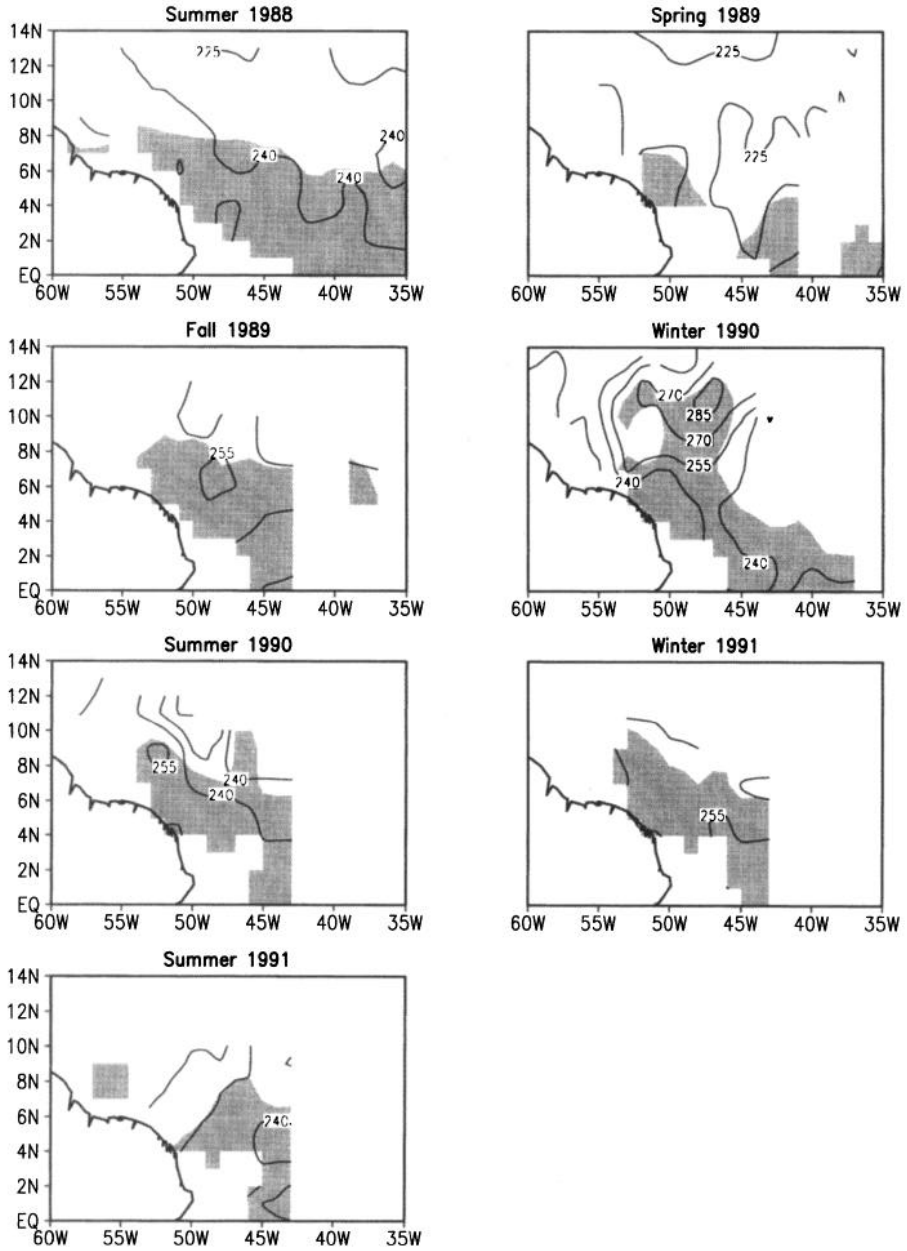

Figure 18. (Continued)

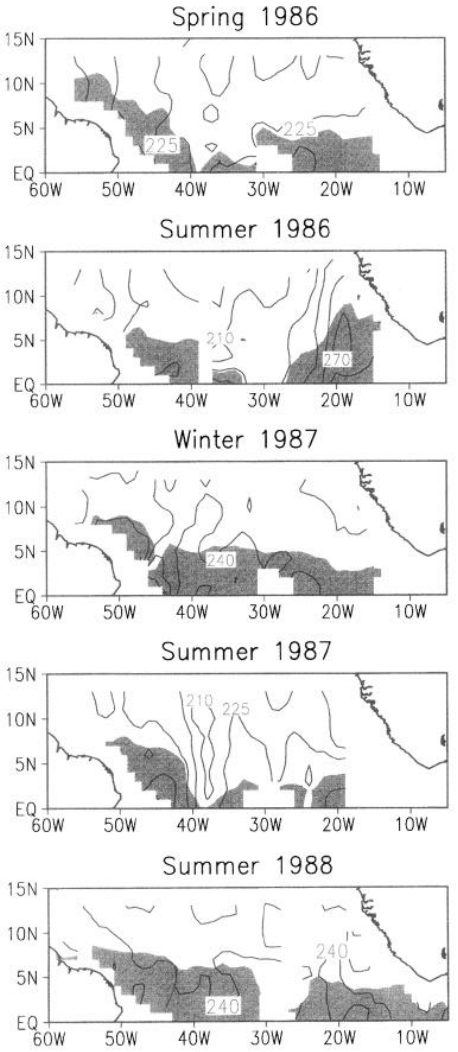

Figure 19. Similar to Figure 18 but for basinwide.

thermocline current developed that, by itself, was responsible for northward transports of 26 Sv. Understanding the causes of this anomalous condition is the subject of ongoing work by our group.

Acknowledgments. We would like to thank V. I. Zaburdaev and E. Shevcheko for their help in correcting the SECTIONS salinity data. We thank the reviewers for a number of useful suggestions. This work has been supported by the National Science Foundation under grant # OCE-9416894 and

the Office of Global Programs/National Oceanographic and Atmospheric Administration under grant # NA66GP0269.

REFERENCES

Bub, F. 1993. The structure of water mass, salt, and temperature transports within intermediate depth of the western tropical Atlantic Ocean, Ph.D. dissertation, University of New Hampshire, Duham, NH, 222 pp.

Bulgakov, N. P., A. S. Vasiliev, V. V. Efimov, G. K. Korotaev, and P. D. Lomakin. 1989. Seasonal deformation of the North Equatorial Countercurrent in the Atlantic Ocean. Morsk. Gidrofiz. Zn., *5,* 12–18.

Candela, J., R. C. Beardsley and R. Limeburner. 1992. Separation of tidal and subtidal currents in ship-mounted acoustic doppler current observations. J. Geophys. Res., *97,* 769–788.

Carton, J. A. and B. Huang. 1994. Warm events in the tropical Atlantic. J. Phys. Oceanogr., *24,* 888–903.

Carton, J. A. and E. J. Katz. 1990. Estimates of the zonal slope and seasonal transport of the Atlantic North Equatorial Countercurrent. J. Geophys. Res., *95,* 3091–3100.

Chepurin, G. A. and J. A. Carton. 1997. Balance mass of the upper layer in the north tropical Atlantic. (manuscript).

Chernova, A. V. and M. V. Chmutov. 1987. The system of storage and treatment of oceanographic data using the OKA data control system. Automated system for collecting and processing oceanographic data. Sevastopol. Preprint MHI, 30 pp.

Cochrane, J. D., F. J. Kelly, Jr. and C. R. Olling. 1979. Subthermocline countercurrents in the western equatorial Atlantic Ocean. J. Phys. Oceanogr., *9,* 724–738.

Defant, A. 1936. Schichtung und Zirkulation des Atlantischen Ozeans. Die Troposphere, *in* Wessenschaftliche Ergebisse der Dentschen Atlantischen Expedition aut dem Forschunss und Vermessungsschiff "Meteor" 1925–1927, 6: 1st. Part, 3, 289–411.

Efimov, V. V. 1987. Main results of hydrographic investigations in the tropical Atlantic EAZO in programme "SECTIONS," *in* Atmosphere, Ocean, Space. Programme "SECTIONS." Moscow.

Fratantoni, D. M., W. E. Johns and T. L. Townsend. 1995. Rings of the North Brazil Current: Their structure and behavior inferred from observations and a numerical simulation. J. Geophys. Res., *100,* 10633–10654.

Friedrichs, M. A. M. and M. M. Hall. 1993. Deep circulation in the tropical North Atlantic. J. Mar. Res., *51,* 697–736.

Gandin, L. S. 1963. Objective Analysis of Meteorological Fields. Gidrometeoizdat. Leningrad.

Garzoli, S. L. and E. J. Katz. 1983. The forced annual reversal of the Atlantic North Equatorial countercurrent. J. Phys. Oceanogr., *13,* 2082–2090.

Garzoli, S. and P. L. Richardson. 1989. Low-frequency meandering of the Atlantic North Equatorial Countercurrent. J. Geophys. Res., *94,* 2079–2090.

Gouriou, Y. and G. Reverdin. 1992. Isopycnal and diapycnal circulation of the upper equatorial Atlantic in 1983–1984. J. Geophys. Res., *97,* 3543–3572.

Henin, C. and P. Hisard. 1987. The North Equatorial Countercurrent observed during the Programme Francais Ocean Climat Dans l'Atlantique Equatorial Experiment in the Atlantic Ocean, July 1982 to August 1984. J. Geophys. Res., *92,* 3751–3758.

Johns, E. and A. M. Wilburn. 1993. Hydrographic observations in the western tropical and subtropical Atlantic Ocean: Atlantic Climate Change Program (ACCP) and Western Tropical Atlantic Experiment (WESTRAX) during 1991 (ERL AOML-23). Atlantic Oceanographic and Meteorology Laboratory, Miami, FL March 1993.

Kalashnikov, P. A. 1985. Primary processing of hydrological data, Gidrometizdat, Leningrad, 152 pp.

Katz, E. J. 1981. Dynamic topography of the sea surface in the equatorial Atlantic. J. Mar. Res., *39,* 53–63.

—— 1993. An Interannual Study of the Atlantic North Equatorial countercurrent. J. Phys. Oceanogr., *23,* 116–123.

Korotaev, G. K. and G. A. Chepurin. 1989. The seasonal variability of large-scale field of current in the northern part of tropical Atlantic. VINITI #4131-B88, Moscow, 50 pp.

Levitus, S. 1994. World Ocean Atlas 1994 CD-Rom Sets. National Oceanographic Data Center Informal Report, *13,* Washington, D.C.

Levitus, S., T. P. Boyer and J. Antonov. 1994. World Ocean Atlas 1994, vol. 5: Interannual variability of upper ocean thermal structure, NOAA Atlas NESDIS 5, U.S. Government Printing Office, Washington, D.C., 150 pp.

Levitus, S. and A. Oort. 1977. A global analysis of oceanographic data. Bull. Am. Met. Soc., *38,* 1270–1284.

McDougall, T. J. 1989. Streamfunction for the lateral velocity vector in a compressible ocean. J. Mar. Res., *47,* 267–284.

Merle, J. 1978. Atlas Hydrologique saisonnier de L'Ocean Atlantique intertropical, Trav. Doc. l'ORSTOM 82, Inst. Francais de Rech. Sci. pour le Dev. en Coop., Paris.

—— 1983. Seasonal variability in the subsurface thermal structure in the tropical Atlantic, *in* Hydrodynamics of the Equatorial Ocean, J. C. J. Nihoul, ed., Elsever, New York, 31–49.

Merle, J. and S. Arnault. 1985. Seasonal variability of the surface dynamic topography in the Atlantic Ocean. J. Mar. Res., *43,* 267–288.

Molinari, R. L. and E. Johns. 1994. Upper layer temperature structure of the western tropical Atlantic. J. Geophys. Res., *99,* 18,225–18,233.

Reverdin, G., R. F. Weiss and W. J. Jenkins. 1993. Ventilation of the Atlantic Ocean Equatorial Thermocline. J. Geophys. Res., *98,* 16,289–16,310.

Richardson, P. L. and G. Reverdin. 1987. Seasonal cycle of velocity in the Atlantic North Equatorial countercurrent as measured by surface drifters, current meters, and ship drifts. J. Geophys. Res., *92,* 3691–3708.

Richardson, P. L. and W. J. Schmitz. 1993. Deep cross-equatorial flow in the Atlantic measured with SOFAR floats. J. Geophys. Res., *98,* 8371–8387.

Roemmich, D. 1983. The balance of geostrophic and Ekman transport in the tropical Atlantic. J. Phys. Oceanogr., *13,* 1534–1539.

Schmitz, W. J. Jr. and P. L. Richardson. 1991. On the sources of the Florida Current. Deep-Sea Res., B38, Suppl 1, S379–S409.

Schott, F. A., L. Stramma and J. Fischer. 1995. The warm water inflow into the western tropical Atlantic boundary regime, spring 1994. J. Geophys. Res., *100,* 24,745–24,760.

Tsuchiya, M., L. D. Talley and M. S. McCartney. 1992. An eastern Atlantic section from Iceland southward across the equator. Deep-Sea Res., *39,* 1885–1917.

Warner, M. J. and R. F. Weiss. 1992. Chlorofluoromethanes in South Atlantic Antarctic Intermediate Water. Deep-Sea Res., *39,* 2053–2075.

Wilson, W. D., E. Johns and R. L. Molinari. 1994. Upper layer circulation in the western tropical North Atlantic Ocean during August 1989. J. Geophys. Res., *99,* 22,513–22,523.

Yoo, J.-M. and J. A. Carton. 1990. Annual and interannual variation of the freshwater budget in the tropical Atlantic Ocean and Caribbean Sea. J. Phys. Oceanogr., *20,* 831–845.

Zhang, H.-M. and N. G. Hogg. 1992. Circulation and water mass balance in the Brazil Basin. J. Mar. Res., *50,* 385–420.

Received: *9 April, 1996;* revised: *27 March, 1997.*